NACA TN 4216

NATIONAL ADVISORY COMMITTEE FOR AERONAUTICS

TECHNICAL NOTE 4216

EFFECT OF FIBER ORIENTATION IN RACES AND BALLS UNDER ROLLING-CONTACT FATIGUE CONDITIONS

By Thomas L. Carter

Lewis Flight Propulsion Laboratory
Cleveland, Ohio

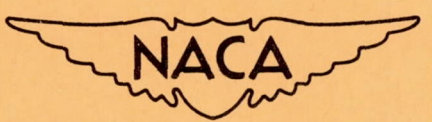

Washington
February 1958

NATIONAL ADVISORY COMMITTEE FOR AERONAUTICS

TECHNICAL NOTE 4216

EFFECT OF FIBER ORIENTATION IN RACES AND BALLS UNDER ROLLING-CONTACT FATIGUE CONDITIONS

By Thomas L. Carter

4697

CX-1

SUMMARY

The effect of fiber orientation on fatigue life was studied for both races and balls in the fatigue spin rig. Three cylindrical race specimens of AISI T-1 tungsten tool steel with controlled fiber orientation were tested under rolling-contact fatigue conditions with 9/16-inch SAE 52100 balls at a maximum theoretical Hertz compressive stress of 750,000 pounds per square inch. A large group of balls with subgroups of ten different materials was also tested at room temperature and a maximum Hertz compressive stress level of 725,000 pounds per square inch.

In both balls and races, a concentration of fatigue failures was observed in that portion of the specimens with the highest angle of intersection of fiber flow lines with the surface. In the races, a continuous trend toward poorer fatigue life from the region of parallel fiber to that of perpendicular fiber orientation was observed. In each of the ball materials studied, the areas of perpendicular fiber orientation (polar areas) were weaker in fatigue than the remainder of the ball.

A significant portion of the nonpolar and nonequatorial failures in the balls appeared to be caused by surface defects which have a relation to the forging lines.

INTRODUCTION

The development and evaluation of new materials for high-temperature bearings require an understanding of the nature and importance of the many factors influencing fatigue life. One major factor influencing this property has been indicated to be the relation of the fiber orientation to the working surface. Reference 1 shows that, in SAE 52100 balls run with randomly oriented tracks, the frequency of failure in the polar areas is about twice that anticipated with a homogeneous material.

Additional information on the influence of fibering created by metal flow during manufacture has been obtained and is reported herein for three reasons:

(1) To study the effect of fiber flow over the entire range of orientations using races with controlled fiber orientation

(2) To improve the statistical confidence in the results of reference 1 by enlarging the ball sample size

(3) To estimate the degree of these orientation effects in balls of several different steel alloys

4697

FIBER ORIENTATION

Any metallic object formed by forging generally possesses a fiber flow pattern which reflects the flow of metal during the forming operation. Since nonmetallic inclusions do not respond to the heat treatment used to control the metallographic structure of the material, they are progressively elongated during each forming operation from the ingot to the final bearing element shape in a manner which reflects the over-all flow of the metal. The desired metallic crystalline structure is obtained by heat treatment, but the inclusions retain their accumulated elongation pattern. This pattern is best described as fiberous in appearance, hence the term "fiber flow lines."

Steel balls as manufactured for bearings are made by upsetting slugs of steel rod between hemispherical dies. The resulting rough ball is heat-treated and then rough and finish ground. This fabrication technique produces a fiber flow pattern with two diametrically opposed areas having fiber orientation approximately perpendicular to the surface. These areas correspond to the ends of the upset rod slug. When excess metal is present, a band of perpendicularly oriented fiber corresponding to the removed flashing at the die parting line is also obtained. The areas in between have fiber orientation approximately parallel to the surface. Thus, the surfaces of balls commonly used in rolling-contact bearings have a pronounced nonhomogeneity with respect to fiber flow orientation. The two areas of perpendicular grain flow are referred to as the poles, while the band of the die parting line is referred to as the equator. The fiber orientation pattern characteristic of balls is illustrated in figure 1.

Bearing races also have a definite fiber flow pattern. Since several methods of manufacture are employed, several characteristic patterns are common. Races ground from seamless tube stock have a fiber flow pattern which is approximately parallel to the race groove, while forged races have a more complicated fiber flow pattern, which usually results in fiber orientation angles ranging from 0° to 90°.

APPARATUS

Only brief descriptions of the apparatus (fig. 2) and procedure are given here. A more detailed presentation can be found in references 1 and 2. Essentially, the rig consists of two balls driven at high speed on the inner surface of a cylinder race by an air jet. Ball loading results from centrifugal force. Speed control and automatic failure shutdown systems are provided.

Specimens with controlled fiber flow orientation were obtained by machining race cylinders from AISI T-1 (18-4-1 tungsten tool steel) billet stock at various angles to the direction of forging. Three cylinders were machined with axes parallel to, at 45° to, and perpendicular to the direction of fiber flow (fig. 3(a)). The first cylinder had fiber orientation parallel to the test surface (fig. 3(b)). The second had fiber orientation ranging continuously from parallel to 45° to the test surface (fig. 3(c)). The third had fiber orientation ranging continuously from parallel to perpendicular to the test surface (fig. 3(d)). The nominal composition and the cleanliness rating of this material are given in table I. Each of the cylinders was hardened to Rockwell C-62 to C-64.

In testing the special race cylinders, about 20 tracks could be run to failure before the cylinder bore was refinished to a 0.120 inch greater internal diameter. The location of a running track was determined by the position of the guide plate assembly vertically in the bore of the test cylinder. Three bore surfaces (3.25, 3.37, and 3.49 diam.) were tested in each cylinder. Sufficient material was removed in each refinishing process to remove any effect of previous stressing. SAE 52100 steel balls, with a fatigue life long enough to ensure that the race failed first, were used in this race evaluation.

The test balls were hardened to Rockwell C-62 to C-64 and were all 1/2 inch in diameter, except the SAE 52100 balls which were 9/16 inch in diameter. The nominal composition and the cleanliness ratings for these groups of balls are given in table I. The running track on the balls was predetermined by randomly grinding two diametrally opposed 1/8-inch flats on the ball surface. All test balls were weighed and inspected at a magnification of 36. The presence of excessive scratches or pitting and any cracks, laminations, or flat spots was noted in a permanent record. Race cylinders for the ball investigation were AISI M-1 (molybdenum type) vacuum-melted tool steel. SAE 10 mineral oil was used as a lubricant in all the tests.

PROCEDURE

Dimensional, surface-finish, and hardness inspections were made prior to test, and care was taken to protect the specimens from mechanical damage and corrosion during handling and storage.

4697 CX-1 back

The bore surface and test balls were coated with the test lubricant during assembly. The rig was brought up to operating speed as rapidly and as smoothly as possible. Approximately 15 milliliters per hour of lubricant were introduced in droplet form into the drive airstream between the guide plates. The atomizing effect of the high-velocity airstream reduced the lubricant to a fine mist which adhered to surfaces to provide a lubricating film. Speed, air pressure, and vibration levels were recorded during the test. Total running time was recorded and converted into total stress cycles on the specimen. A post-test surface examination at a magnification of 36 was made to observe track conditions.

Failure life data for the race cylinder specimens were plotted on Weibull paper, which is a distribution of the log log of the reciprocal of the portion of the sample surviving against the log of stress cycles to failure. The location of the failures in the special race cylinder specimens was noted with respect to fiber flow direction.

The ball specimens were etched with 60 percent hydrochloric acid at 160° F after testing to reveal the polar areas and the location of failure with respect to the poles.

RESULTS AND DISCUSSION

Race Data

0° Cylinder. - The 0° cylinder (fig. 3(b)) was tested as a basis for comparison with the cylinders which had a range of fiber orientation. Fifty-seven fatigue failures were produced with this specimen. A chart of the failure locations is given in figure 4. The data show a random failure pattern. These results might be anticipated since the bore surface is homogeneous with respect to fiber orientation, metallographic structure, hardness, and chemical composition.

Since any weakness or unusual strength in the specimen would affect life as well as position of fatigue failures, the lives of the fatigue failures were tabulated. A Weibull plot for the first 50 of the 57 failures in the 0° cylinder is given in figure 5. It was convenient to use only the first 50 failures because median rank tables (ref. 3) used to find the ordinate in the Weibull plot were readily available only to sample sizes of 50. With this large sample size the plot should be practically coincident with that which would result when using a sample size of 57.

0° to 90° Cylinder. - A chart of the 67 failures for this cylinder is given in figure 6(a). Because the bore surface has four quadrants with the 0° to 90° range of controlled fiber orientation (fig. 3(d)), the data were condensed into one equivalent first quadrant. The condensed data are given in figure 6(b). Examination of this chart shows an apparent increase

4697

in failure density in the region of higher angles of intersection of fiber flow with the bore surface. A measure of this preferred location of fatigue failures with respect to fiber flow orientation is possible by dividing the 90° range into zones and counting the number of failures in each zone.

The greatest number of divisions which gave a continuous trend is five zones of 18° each as shown in figure 7. A definite trend toward a concentration of failures at the higher fiber orientation angles is shown. When using 18° zones, the failure density in the zone closest to perpendicular fiber orientation is approximately three times the failure density in the zone near parallel fiber orientation.

A cumulative distribution will give a continuous measure of failure susceptibility over the 0° to 90° range. In a homogeneous material this distribution would be a straight line as the failures accumulated at a constant rate over the range. This is shown in figure 8 for comparison with the experimental results.

The lives of fatigue failures for this cylinder were tabulated and are presented as a Weibull plot in figure 9. As for the 0° cylinder, only the first 50 failures are presented.

0° to 45° Cylinder. - Sixty-four fatigue failures were produced with the 0° to 45° cylinder (fig. 3(c)). The locations of the failures are given in figure 10(a). As in the 0° to 90° cylinder, four identical quadrants are present so the data were condensed into one equivalent first quadrant (fig. 10(b)). A preference for failures to locate near the highest angle of fiber orientation is observed. It will be noted that the abscissa scale in figure 10(b) is nonlinear. This is so because in the 0° to 45° cylinder equal ranges of fiber orientation angle represented progressively larger areas on the test cylinder from lower to higher angles of fiber orientation. Figure 10(b) presents an undistorted plot of the 0° to 45° cylinder bore condensed into one quadrant, thus the scale of fiber orientation angle is nonlinear. An analysis of these data on the basis of equal increments of fiber orientation angle would have to take this uneven distribution of area into consideration.

Figure 11 is a plot of the number of failures in four equal zones of fiber orientation adjusted to compensate for the unequal area in each zone. As in the 0° to 90° cylinder, this 0° to 45° cylinder gives an increase in failure density for the region closest to the highest fiber orientation angle. The range between highest and lowest density is less than that for the 0° to 90° cylinder, but this might be expected since the range of orientation angles is only half that in the 0° to 90° cylinder.

A cumulative distribution of failures against fiber orientation, adjusted for area, is given in figure 12. In this plot the number of

4697

failures accumulates at rates less than are expected for a homogeneous material at low angles and accelerates to a rate of failure greater than that in a homogeneous material toward the greater fiber orientation angles. The theoretical curve for a homogeneous material is not a straight line because equal increments of fiber orientation angle do not represent equal areas. This is another indication that the region of higher fiber orientation angles is more susceptible to rolling-contact fatigue failure than a region with lower fiber orientation angles.

The fatigue lives observed with this cylinder specimen were tabulated and are presented as a Weibull plot in figure 13. As before, only the first 50 failures were used.

Discussion of Race Data

The position of fatigue failures with respect to fiber orientation angle in both the 0° to 90° and the 0° to 45° test cylinders indicates a tendency for failures to occur preferentially in regions where the angle between the fiber direction and the surface is the greatest. In the 0° to 90° cylinder about three times as many failures occurred in the zone from 72° to 90° fiber orientation as in the zone of equal area from 0° to 18° fiber orientation. In the 0° to 45° cylinder about twice the failure density existed in a zone near the 45° fiber compared with an equivalent zone round the 0° fiber. In the 0° cylinder where all fiber was parallel to the surface, failure locations appeared to be randomly located.

A greater than average failure density is an indication that a region is weak in fatigue strength. Thus, the running time (i.e., stress cycles) to failure should be shorter for the region where failure density is the greatest. The Weibull plots of the fatigue lives of the three cylinders are compared in figure 14.

The 0° cylinder has the best life, while the 0° to 90° cylinder has the poorest life. However, the difference in life for the 0° to 90° and the 0° to 45° cylinders appears to be negligible. It should be noted that the 0° to 90° cylinder contained billet core material (fig. 3(a)), while the 0° cylinder did not. Since core material is often dirtier than the surrounding metal, it was thought that this might account for the difference in lives. Accordingly, the bore of the 0° to 90° cylinder was divided into three axial zones (one including the billet axis), and life plots were made for the lower, center, and upper thirds. The zone lives were practically coincident with the over-all life. For the center zone containing the core material, the 10- and 50-percent lives were 3×10^6 and 13×10^6 stress cycles, respectively, while the corresponding lives for the over-all cylinder were 3.1×10^6 and 13.2×10^6 stress cycles.

The 0° cylinder has a 50 percent greater life at the 10-percent failure point than the 0° to 90° cylinder. These life data are consistent with the failure-density data.

The previous discussion presents a direct presentation of the life data for the three cylinders but does not give a quantitative measure of the variation in life between the extremes of parallel and perpendicular grain. The Weibull plot for the 0° cylinder is a measure of life for parallel fiber, but that for the 0° to 90° cylinder represents a composite value for a range of orientations. A Weibull plot for the portion of the 0° to 90° cylinder with fiber orientations near the perpendicular would give a more representative value. Such a plot is given in figure 15 for the zone representing fiber orientation angles from 81° to 90°. As expected, the 10-percent failure life is lower than that for the cylinder as a whole. This plot is not entirely correct statistically since a failure in the remainder of the cylinder would be a runout in the zone under consideration. However, five of the six lowest lived failures occurred in the 81° to 90° zone. Figure 15 was drawn using a sample size of six with five failures and one runout. This procedure should give a fair estimate of the 10-percent life for this zone.

In figures 14 and 15 life data are given for specimens with ranges of fiber orientation angles of 0°, 0° to 45°, 0° to 90°, and 81° to 90°, which have average values of 0°, 27.5° (adjusted), 45°, and 85.5°, respectively. Thus, since a plot of life against average fiber orientation angle is possible, figure 16 presents 10-percent life plotted against average fiber orientation angle. The trend toward lower life at higher fiber orientation angles is quite consistent. Extrapolation of this plot to perpendicular fiber gives a ratio between parallel fiber life and perpendicular fiber life of the order of 4 to 1.

Ball Data

A large group of balls, of which 211 failed, was tested with randomly oriented tracks and was used to obtain data on failure location with respect to fiber orientation. The large sample size assured random orientation. Post-test etching showed that about 63 percent of the tracks (in both the failed and unfailed balls) ran through the poles, which is in good agreement with the 64-percent theoretical value derived in reference 1. This sample group consisted of subgroups of ten different materials.

Since the tracks of the balls were randomly oriented with respect to fiber orientation, a random failure pattern should have been produced if the balls were of uniform fatigue strength over the entire surface area. Reference 1 contains a computation of the probability of failure occurring in a polar area under various limiting conditions. Table II is a comparison of the actual failure locations with the theoretical (15.0 percent)

results anticipated. The ratio of experimental to theoretical results is given only for the samples which showed an approximately random track orientation, for example, 63 percent of the total of the failed tracks passing through the polar areas. For the entire group the proportion of polar failures (30.8 percent) is approximately two times that which could be expected if the entire ball surface had uniform fatigue strength. The proportion of nonpolar failures is correspondingly smaller than that predicted theoretically. This susceptibility of polar areas to failure indicates that the polar areas are significantly weaker in fatigue. The tendency for a larger than normal proportion of polar failures seems to hold for each of the ten individual materials investigated although some of the smaller samples were not randomly oriented and thus are difficult to analyze. A metallographic cross section of a typical polar failure is given in figure 17.

Table III gives the distribution of failures in the 144 balls, taken from the 211 in table II, which ran over the poles. If the balls were of uniform fatigue strength, the portion of failures occurring in the poles would be equal to the ratio of the statistically averaged track length occurring within the poles to the total track length (23.4 percent). For the total group of balls the actual result (45 percent) was about 1.9 times that number. For each of the ten ball materials studied, the polar areas appear to be weak in fatigue because for each material the ratio of actual to theoretical fraction of polar failures is greater than unity.

Figure 18 is a plot of failure density on the ball surface as a function of the elevation from the equator toward the pole (i.e., ball latitude). This figure was compiled from the failure position data obtained from the 211 balls examined. The data were plotted by counting all the failures in each of nine 10° zones of ball latitude and dividing by a factor equal to the percentage of the total ball area in the zone. This gave a failure density for each zone. This plot shows a very marked increase in the density of failures at higher ball latitude, that is, the polar areas where the fiber orientation is approximately perpendicular. The area near the equator also has a significant increase in failure density. This area also has perpendicular fiber orientation due to the removal of flashing formed at the upsetting die parting line. These characteristic fiber orientation areas are illustrated in figure 1. A plot such as figure 18 for a homogeneous material would present a uniform band of failure density.

A significant portion of the fatigue failures occurring outside the poles and equator also exhibited a unique appearance which is apparently tied in with the fiber flow pattern originating in the upset forging of the balls. In this area the fiber orientation is parallel to the surface, but open discontinuities which are perpendicular to the equator (die parting line) are frequently observed during post-test inspection at high magnification (ref. 1). Any such defects near the surface would cause

stress concentrations and accelerate fatigue failure. Figure 19 shows this condition for one ball each of AISI M-1, AISI M-10, AISI T-1, and SAE 52100. In each case the failure occurred at an inclusion which was at an angle to the running track but perpendicular to the equator. This condition was observed in approximately 30 percent of the balls which failed outside the poles. No correlation with the angle of track and inclusion intersection was found. In most cases the inclusion was observed in the preinspection and post inspection. The photographs in figure 19 were taken after etching in order to reduce the technical difficulties involved in photographing a polished curved surface.

All failures observed in this series were similar to each other and resembled those characteristic of full-scale bearings (fig. 20). They were limited in area and depth of spalling and appeared to originate from subsurface shear cracking. A comparison of a typical fatigue failure from the spin rig with a bearing race failure is given in figure 20.

4697

CX-2

SUMMARY OF RESULTS

Three AISI T-1 tungsten tool-steel race cylinder specimens with controlled fiber orientation were tested under rolling-contact fatigue conditions with 9/16-inch SAE 52100 balls at room temperature and a maximum Hertz compressive stress level of 750,000 pounds per square inch. A large group of balls with subgroups of ten different materials was tested under rolling-contact fatigue conditions at room temperature and a maximum Hertz compressive stress level of 725,000 pounds per square inch. The results of these studies are as follows:

1. In both balls and races a concentration of fatigue failures was observed in that portion of the specimens with the greatest angle of intersection of fiber flow lines with the surface. Thus, the polar or end grain areas of the balls were significantly weak in fatigue. A somewhat lesser weakness was observed for the equator area.

2. A continuous trend toward lower fatigue life was observed with the race specimens in the range from parallel to perpendicular fiber orientation.

3. In the balls a significant portion of the nonpolar and nonequatorial failures appeared to be caused by surface defects having a relation to the forging lines.

4. Fiber orientation effects appeared to influence fatigue failure in a similar manner for all the ball materials studied.

Lewis Flight Propulsion Laboratory
National Advisory Committee for Aeronautics
Cleveland, Ohio, November 25, 1957

REFERENCES

1. Butler, Robert H., Bear, H. Robert, and Carter, Thomas L.: Effect of Fiber Orientation on Ball Failures Under Rolling-Contact Conditions. NACA TN 3933, 1957.

2. Macks, E. F.: The Fatigue Spin Rig - A New Apparatus for Rapidly Evaluating Materials and Lubricants for Rolling Contact. Lubrication Eng., vol. 9, no. 5, Oct. 1953, pp. 254-258.

3. Johnson, Leonard G.: The Median Ranks of Sample Values in Their Population with an Application to Certain Fatigue Studies. Ind. Math., vol. 2, 1951, pp. 1-9.

4697

TABLE I. - ANALYSIS AND CLEANLINESS OF SPECIMENS

Material	ASTM Cleanliness		Analysis (specified)									
	A-	D-	C	P	S	Mn	Si	Al	Cr	V	W	Mo
SAE 52100 (air-melt)	1	1	1.00	0.025 max.	0.025 max.	0.35	0.28	----	1.45	----	-----	----
AISI M-1 (air-melt)	1	1	0.80	0.030 max.	0.030 max.	0.23	0.23	----	4.00	1.00	1.50	8.50
MHT (air-melt)	1	1	0.98	0.025 max.	0.025 max.	0.40	0.54	1.25	1.38	----	-----	----
TMT (air-melt)	1	1	1.00	0.025 max.	0.025 max.	0.50	1.00	0.08	1.45	----	-----	0.30
AISI M-10 (air-melt)	1	1	0.85	0.030 max.	0.030 max.	0.23	0.30	----	4.00	2.00	-----	8.00
Halmo (vacuum-melt)	1	1	0.65	0.030 max.	0.030 max.	0.27	1.20	----	4.72	0.55	-----	5.36
AISI T-1 (air-melt)	1	1	0.70	0.030 max.	0.030 max.	0.30	0.25	----	4.00	1.00	18.00	----
AISI MV-1 (air-melt)	1	1	0.80	0.030 max.	0.030 max.	0.30	0.25	----	4.10	1.10	-----	4.25
AISI M-50 (air-melt)	1	1	0.80	0.030 max.	0.030 max.	0.30	0.25	----	4.00	1.10	-----	4.0
AISI M-1 (vacuum-melt)	1	1	0.80	0.030 max.	0.030 max.	0.23	0.23	----	4.00	1.00	1.50	8.50
AISI T-1 (air-melt), cylinders	1	1	0.70	0.030 max.	0.030 max.	0.30	0.25	----	4.00	1.00	18.00	----

4697 CX-2 back

TABLE II. - EXPERIMENTAL AND THEORETICAL FAILURE LOCATION DISTRIBUTIONS IN RANDOMLY ORIENTED BALLS[a]

Material	Location of failures	Experimental results		Theoretical fraction of failures (b)	Ratio of experimental to theoretical results
		Number of failures	Fraction of failures		
SAE 52100,[c] 9/16" Diam.	Polar area	14	0.326	0.15	2.17
	Nonpolar	29	.674	.85	.79
AISI M-1, 1/2" Diam.	Polar area	15	0.205	0.15	1.37
	Nonpolar	58	.795	.85	.94
AISI M-1 (vacuum-melt), 1/2" Diam.	Polar area	3	0.231	0.15	1.54
	Nonpolar	10	.769	.85	.90
AISI MV-1, 1/2" Diam.	Polar area	5	0.217	0.15	1.45
	Nonpolar	18	.783	.85	.92
AISI M-10, 1/2" Diam.	Polar area	4	0.444	0.15	(d)
	Nonpolar	5	.556	.85	
AISI M-50, 1/2" Diam.	Polar area	5	0.417	0.15	(d)
	Nonpolar	7	.583	.85	
MHT, 1/2" Diam.	Polar area	2	0.167	0.15	1.11
	Nonpolar	10	.833	.85	.98
TMT, 1/2" Diam.	Polar area	10	0.833	0.15	(d)
	Nonpolar	2	.167	.85	
Halmo, 1/2" Diam.	Polar area	5	0.500	0.15	(d)
	Nonpolar	5	.500	.85	
AISI T-1, 1/2" Diam.	Polar area	2	0.500	0.15	(d)
	Nonpolar	2	.500	.85	
Total	Polar area	65	0.308	0.15	2.05
	Nonpolar	146	.692	.85	.81

[a]All groups had an average pole half-angle of 40°.

[b]For a homogeneous material as calculated in ref. 1.

[c]Includes 29 failures reported in ref. 1.

[d]Computations omitted because track orientation was not approximately random.

4697

TABLE III. - DISTRIBUTION OF FAILURES IN RANDOMLY ORIENTED BALLS WHICH RAN OVER POLAR AREAS[a]

Material	Location of failures	Experimental results		Theoretical fraction of failures (b)	Ratio of experimental to theoretical results
		Number of failures	Fraction of failures		
SAE 52100,[c] 9/16" Diam.	Polar area	14	0.560	0.234	2.39
	Nonpolar	11	.440	.766	.57
AISI M-1, 1/2" Diam.	Polar area	15	0.300	0.234	1.28
	Nonpolar	35	.700	.766	.97
AISI M-1 (vacuum-melt), 1/2" Diam.	Polar area	3	0.375	0.234	1.60
	Nonpolar	5	.625	.766	.82
AISI MV-1, 1/2" Diam.	Polar area	5	0.385	0.234	1.65
	Nonpolar	8	.615	.766	.80
AISI M-10, 1/2" Diam.	Polar area	4	0.572	0.234	2.44
	Nonpolar	3	.428	.766	.56
AISI M-50, 1/2" Diam.	Polar area	5	0.556	0.234	2.37
	Nonpolar	4	.444	.766	.58
MHT, 1/2" Diam.	Polar area	2	0.286	0.234	1.22
	Nonpolar	5	.714	.766	.93
TMT, 1/2" Diam.	Polar area	10	0.833	0.234	3.56
	Nonpolar	2	.167	.766	.22
Halmo, 1/2" Diam.	Polar area	5	0.500	0.234	2.14
	Nonpolar	5	.500	.766	.65
AISI T-1, 1/2" Diam.	Polar area	2	0.667	0.234	2.85
	Nonpolar	1	.333	.766	.44
Total	Polar area	65	0.451	0.234	1.93
	Nonpolar	79	.549	.766	.72

[a]All groups had an average pole half-angle of 40°.

[b]For a homogeneous material as calculated in ref. 1.

[c]Includes 16 failures from ref. 1.

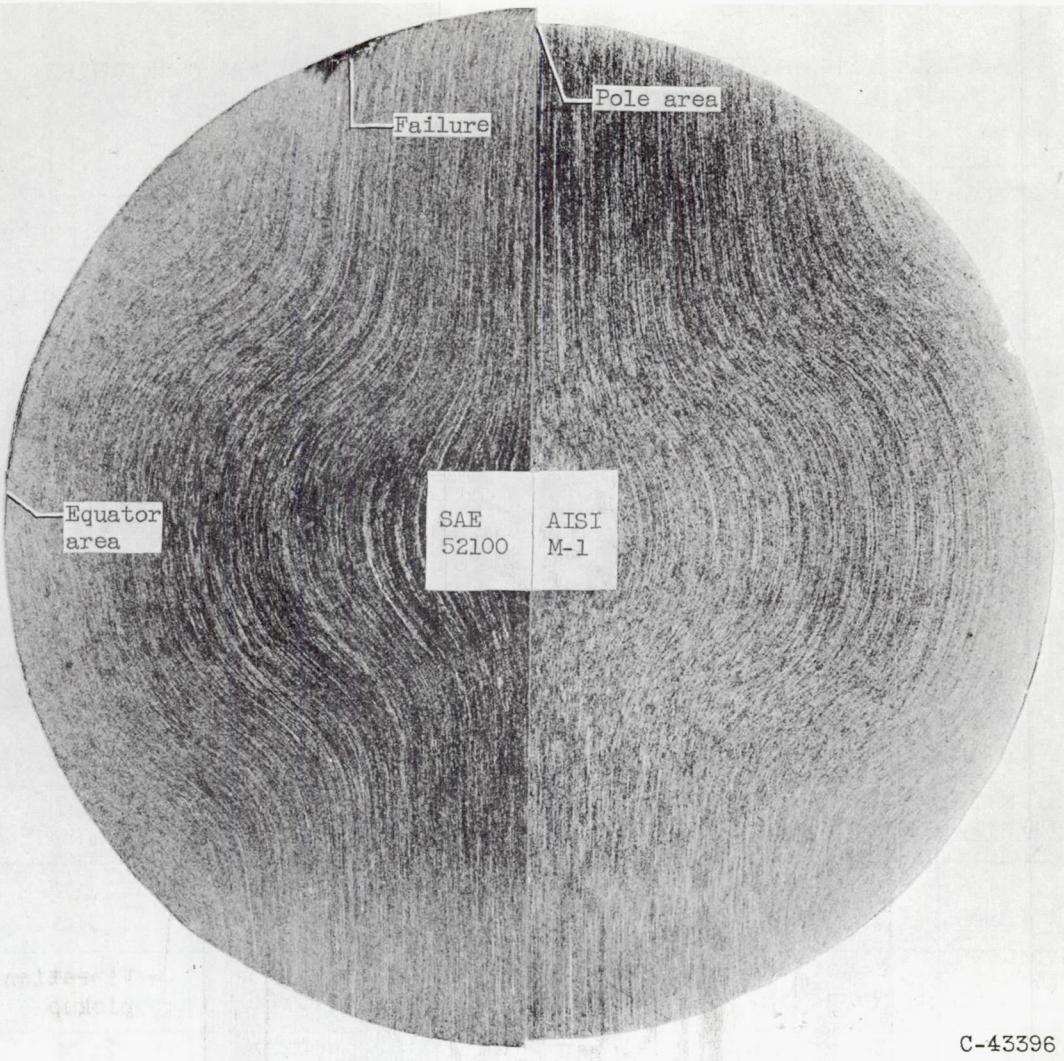

(a) Cross sections showing fiber orientation.

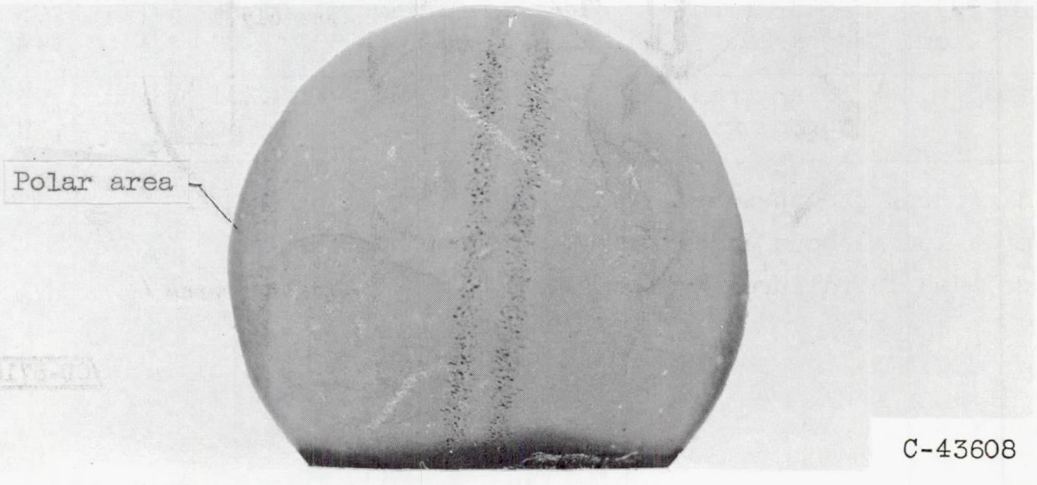

(b) Poles and equator.

Figure 1. - Fiber orientation on SAE 52100 and AISI M-1 balls.

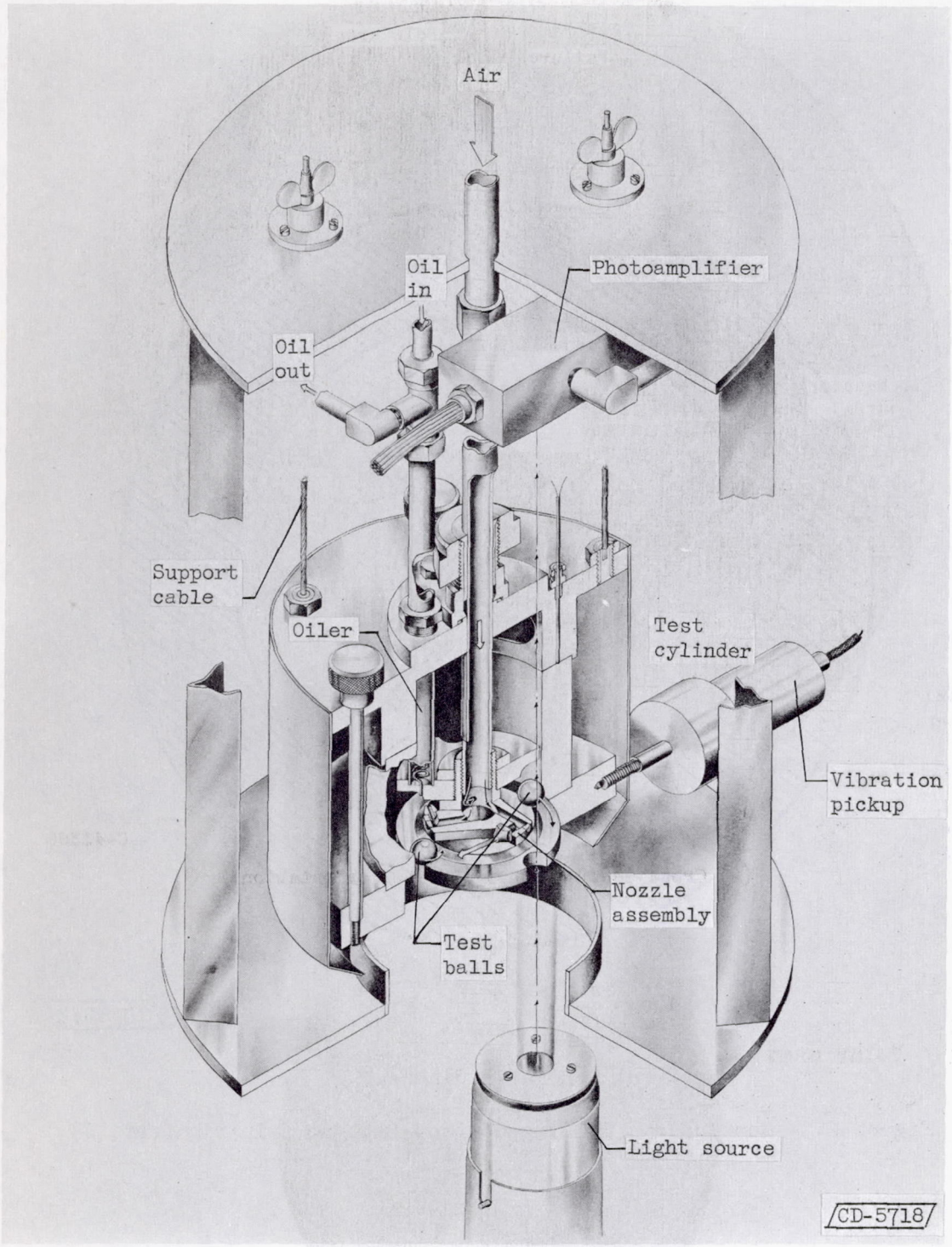

(a) Cutaway view.

Figure 2. - Rolling-contact fatigue spin rig (ref. 1).

4697

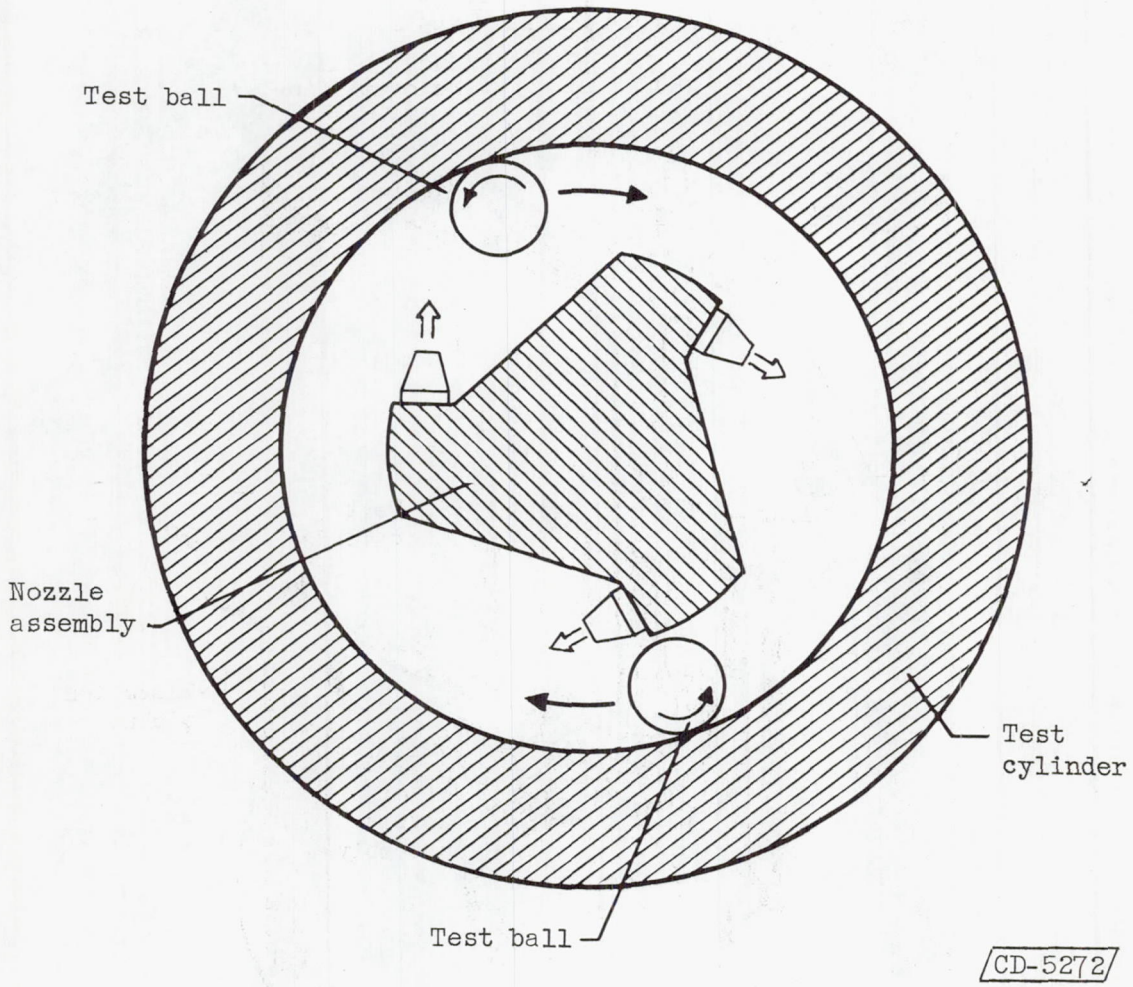

(b) Schematic diagram.

Figure 2. - Concluded. Rolling-contact fatigue spin rig (ref. 1).

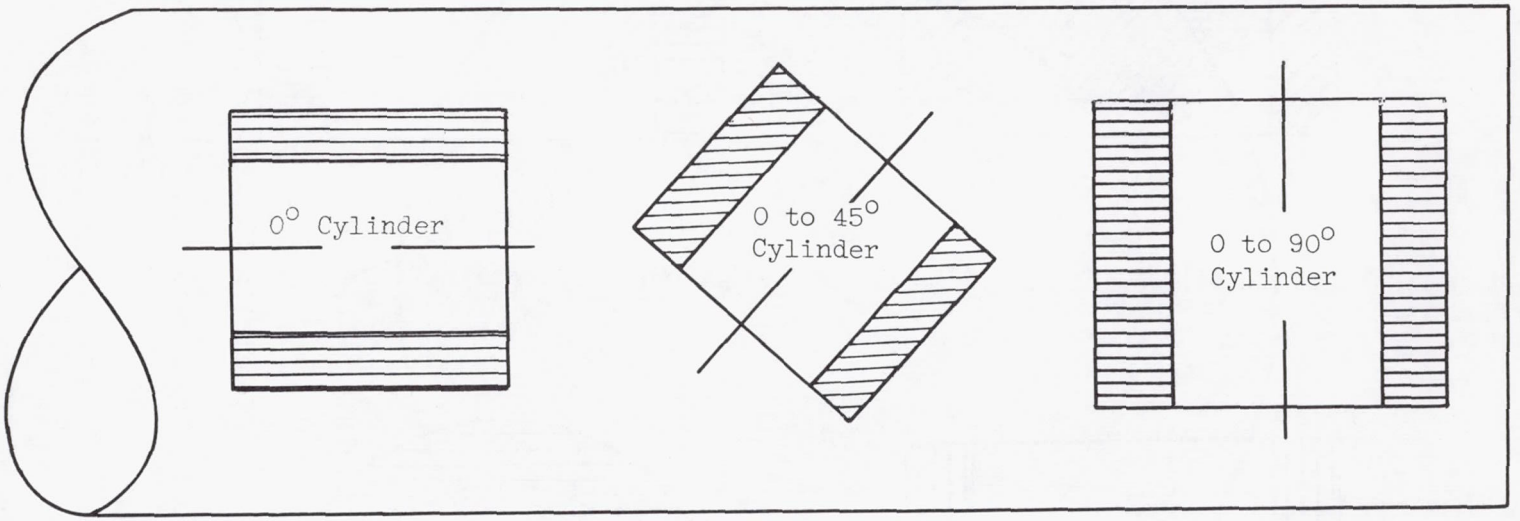

(a) Cylinder orientation in billet stock.

Figure 3. - Fiber orientation in race cylinders.

4697

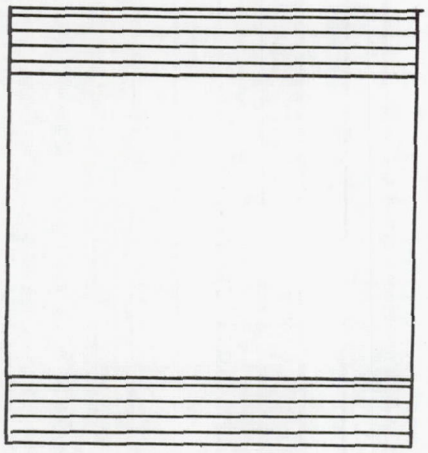

(b) 0° Cylinder.

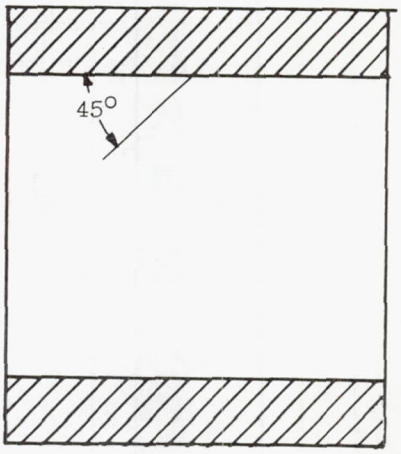

(c) 0° to 45° Cylinder.

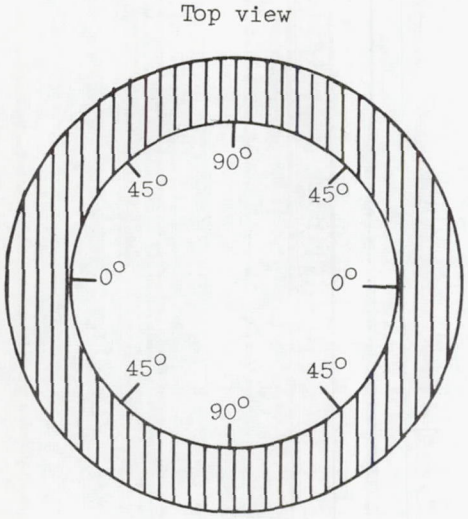

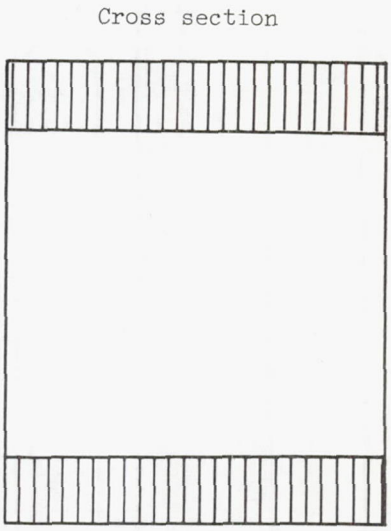

(d) 0° to 90° Cylinder.

Figure 3. - Concluded. Fiber orientation in race cylinders.

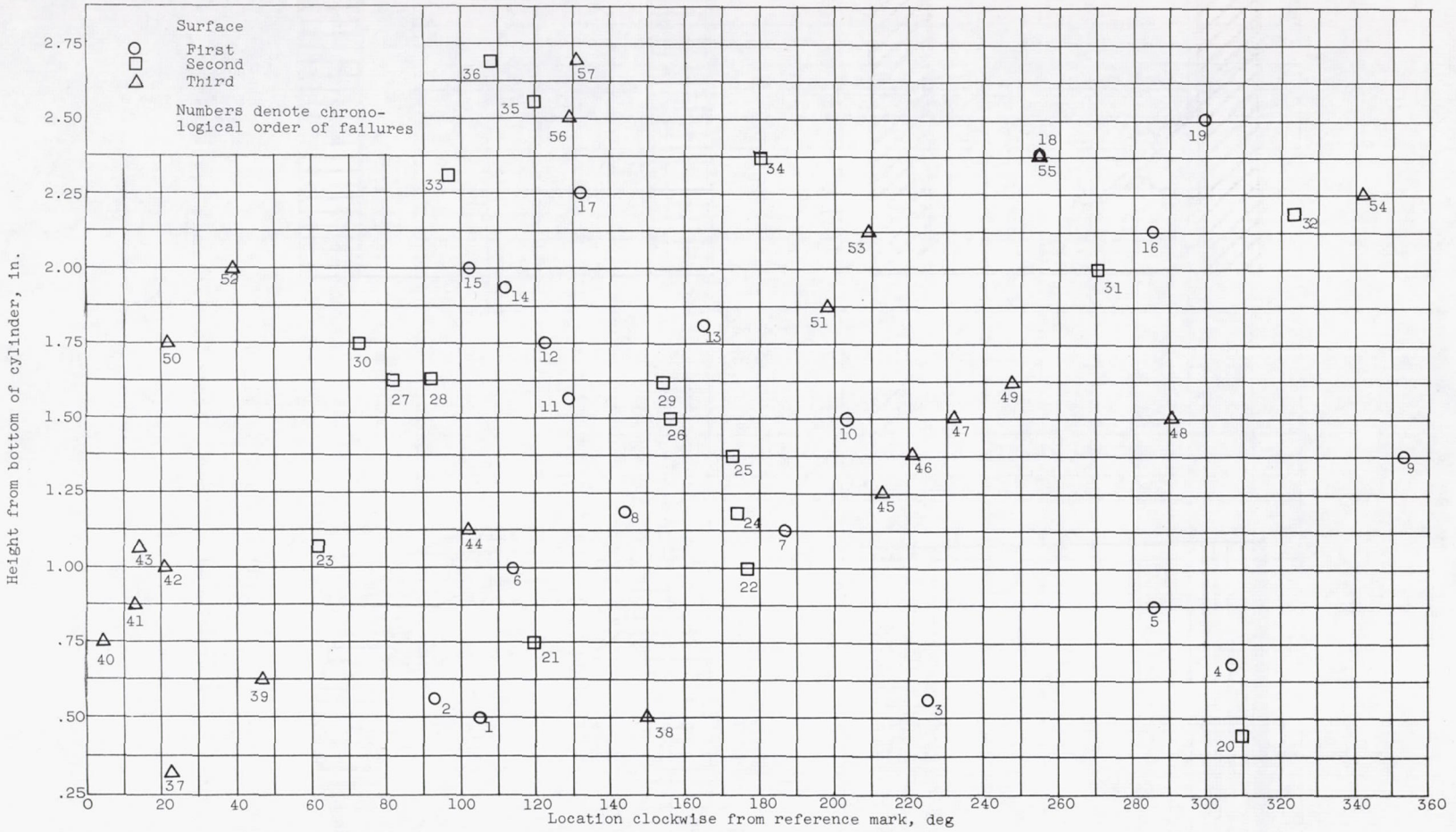

Figure 4. - Failure locations in 0° cylinder.

4697

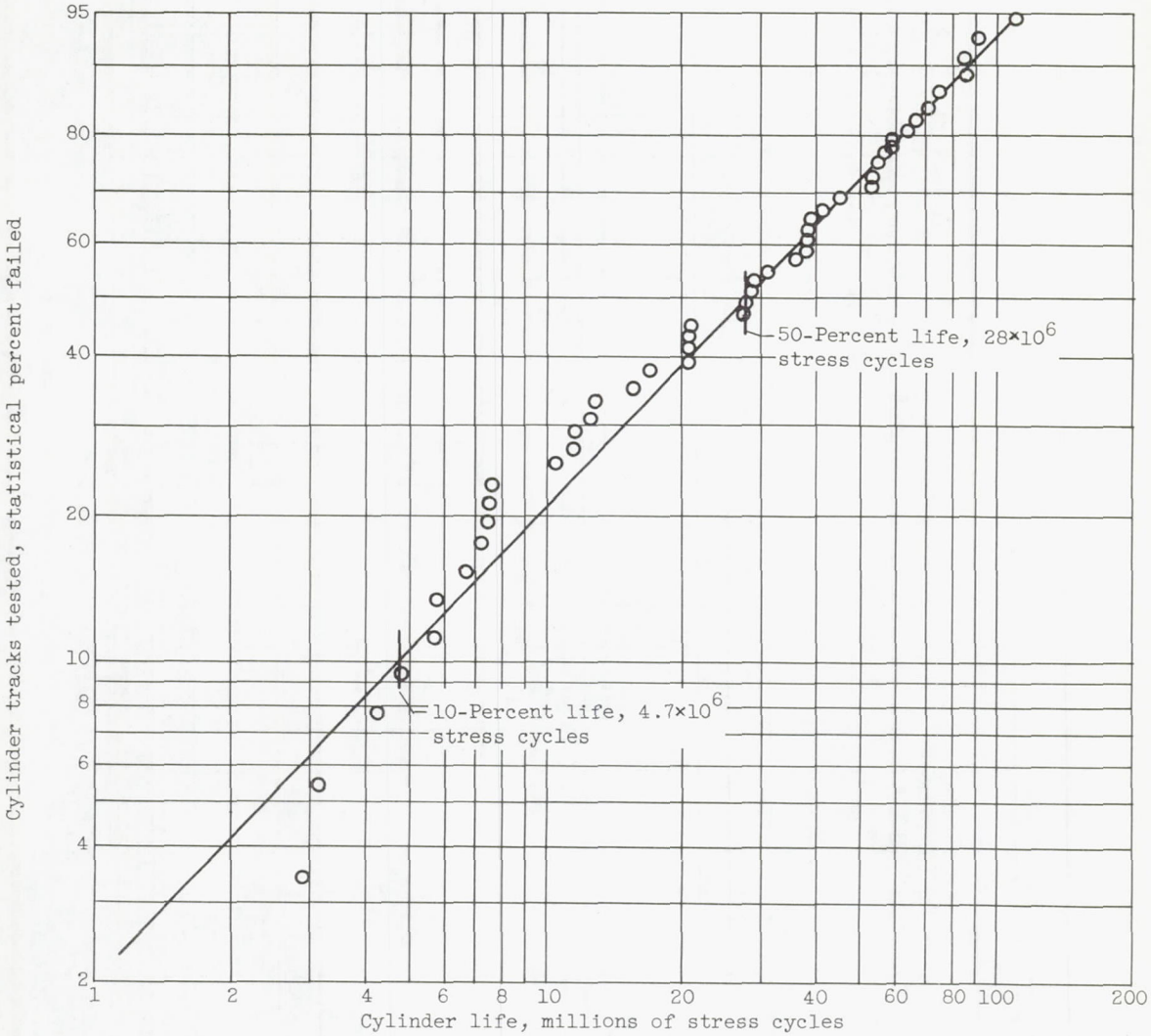

Figure 5. - Fatigue life of 0° cylinder at room temperature. Lubricant, SAE 10 mineral oil; maximum Hertz compressive stress, 750,000 pounds per square inch.

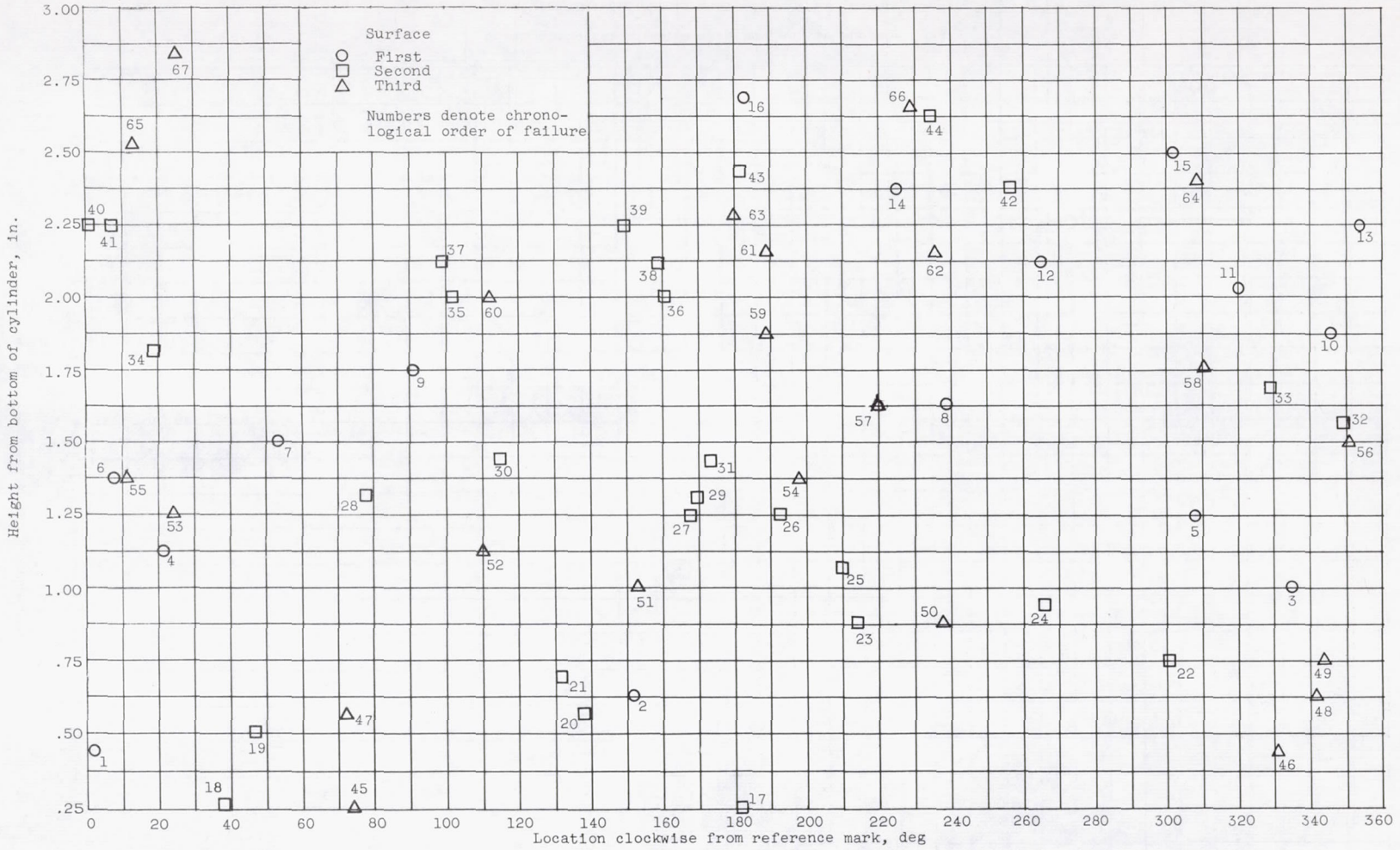

(a) Four quadrants.

Figure 6. - Failure locations in 0° to 90° cylinder.

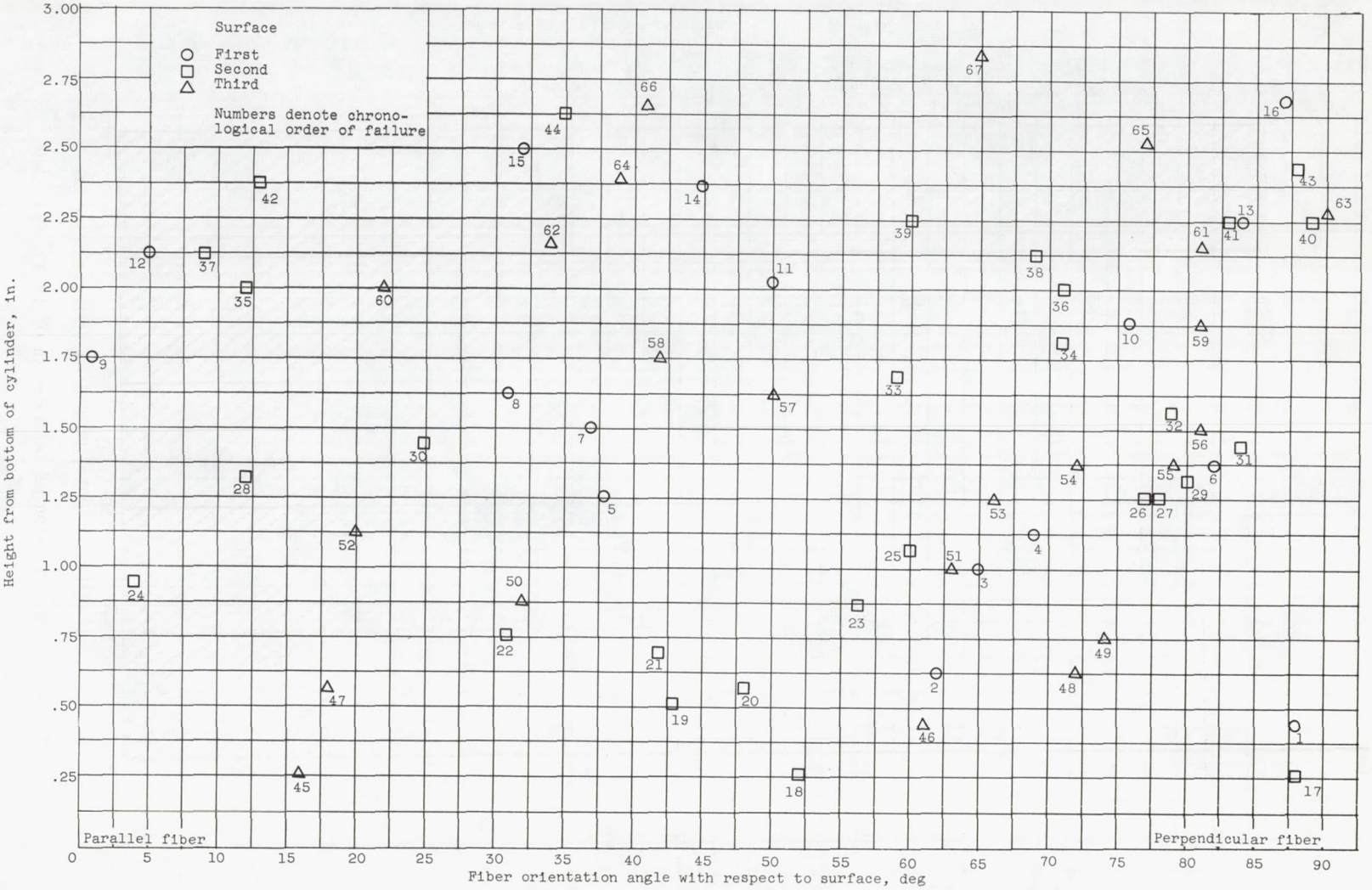

(b) Condensed into an equivalent first quadrant.

Figure 6. - Concluded. Failure locations in 0° to 90° cylinder.

4697

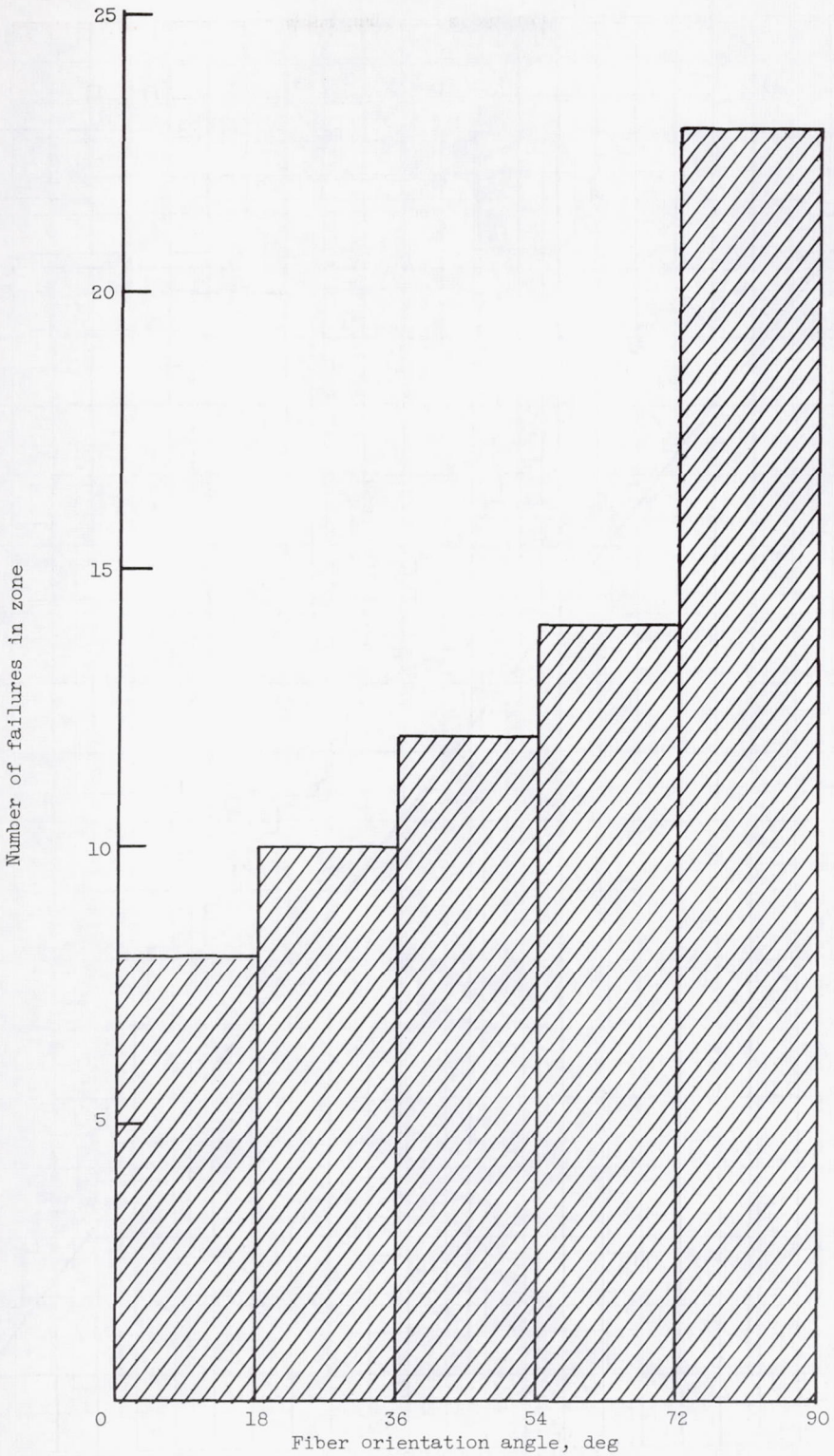

Figure 7. - Distribution of failures in 0° to 90° cylinder.

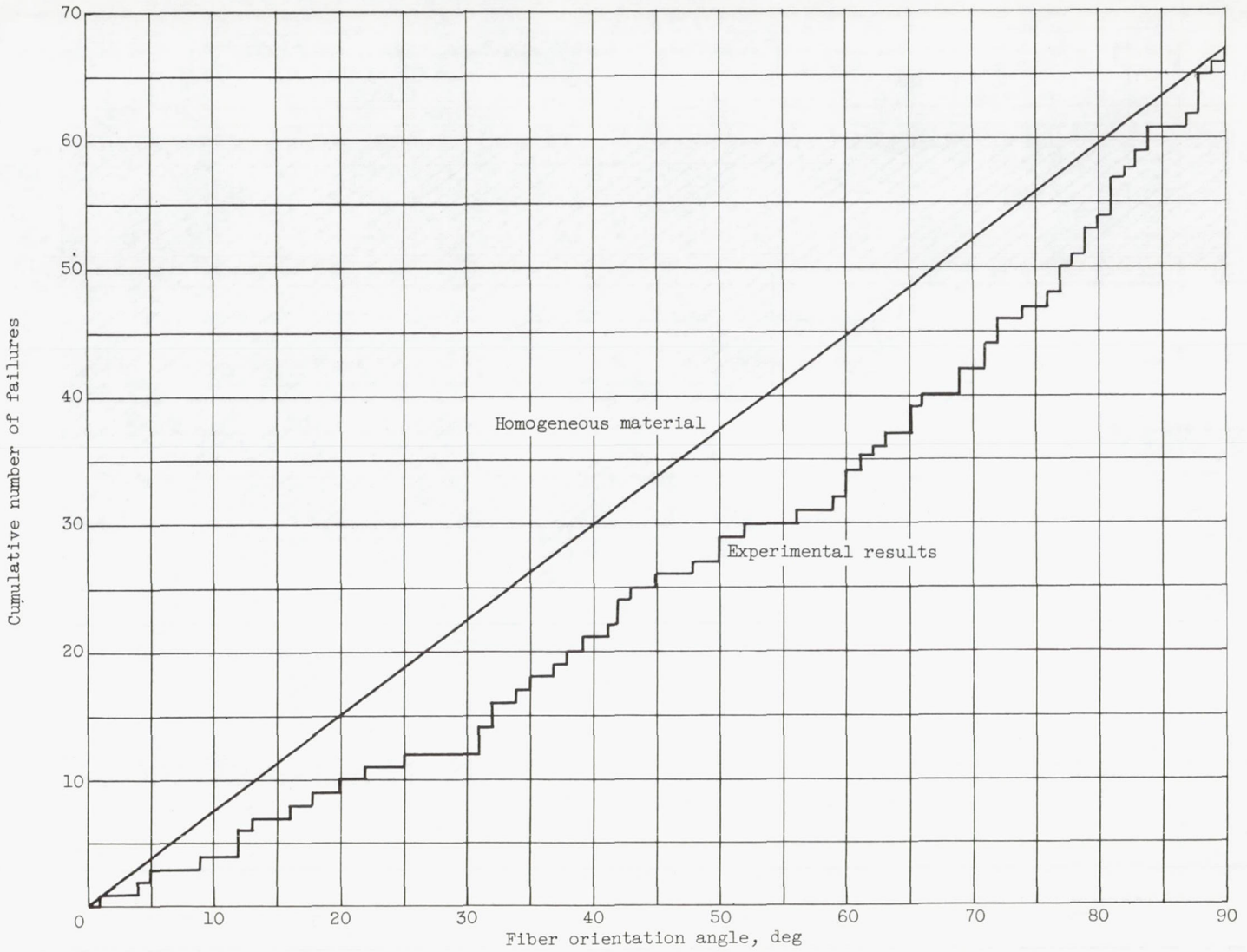

Figure 8. - Cumulative failure distribution in 0° to 90° cylinder.

4697
CX-4

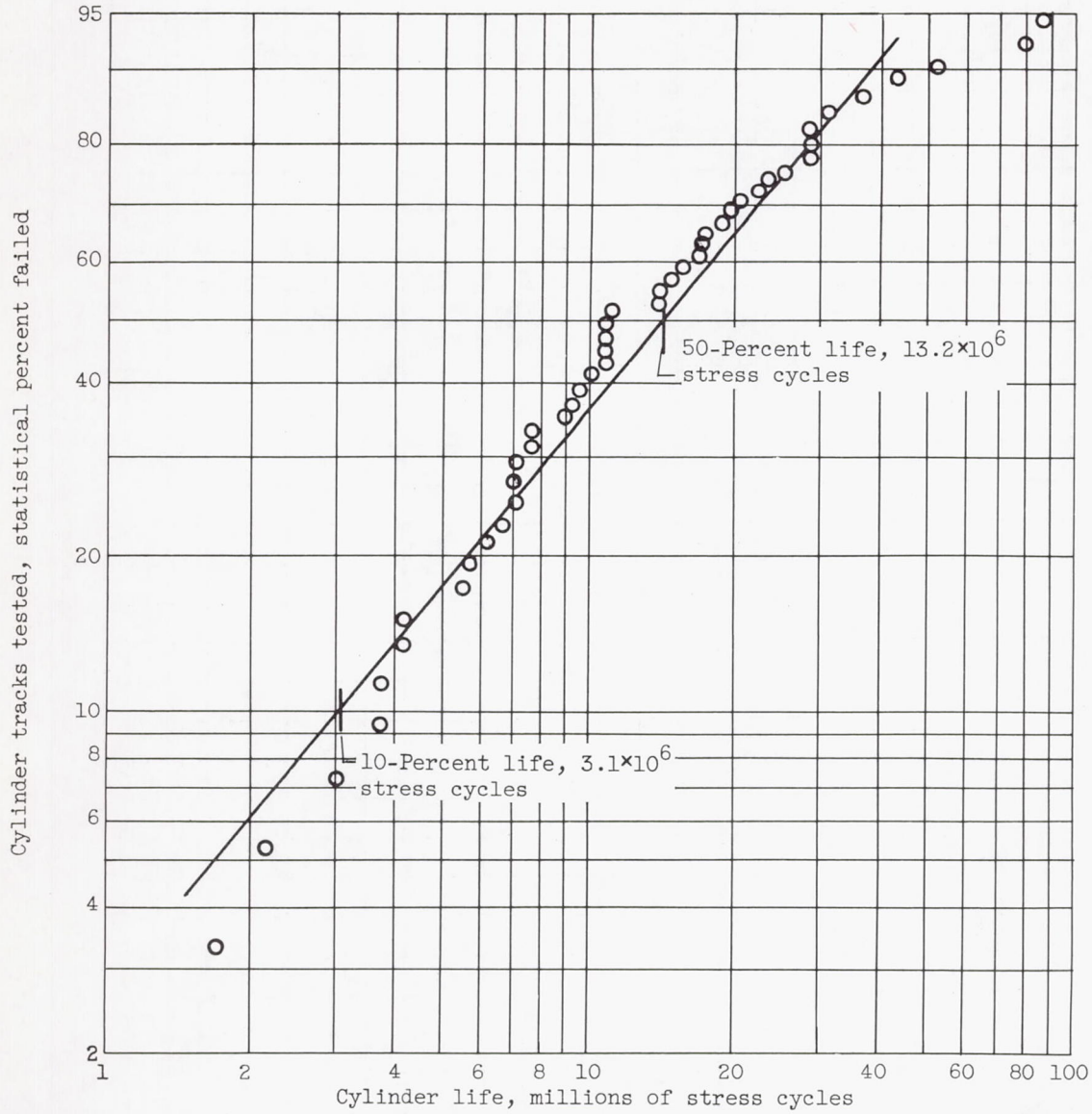

Figure 9. - Fatigue life of 0° to 90° cylinder at room temperature. Lubricant, SAE 10 mineral oil; maximum Hertz compressive stress, 750,000 pounds per square inch.

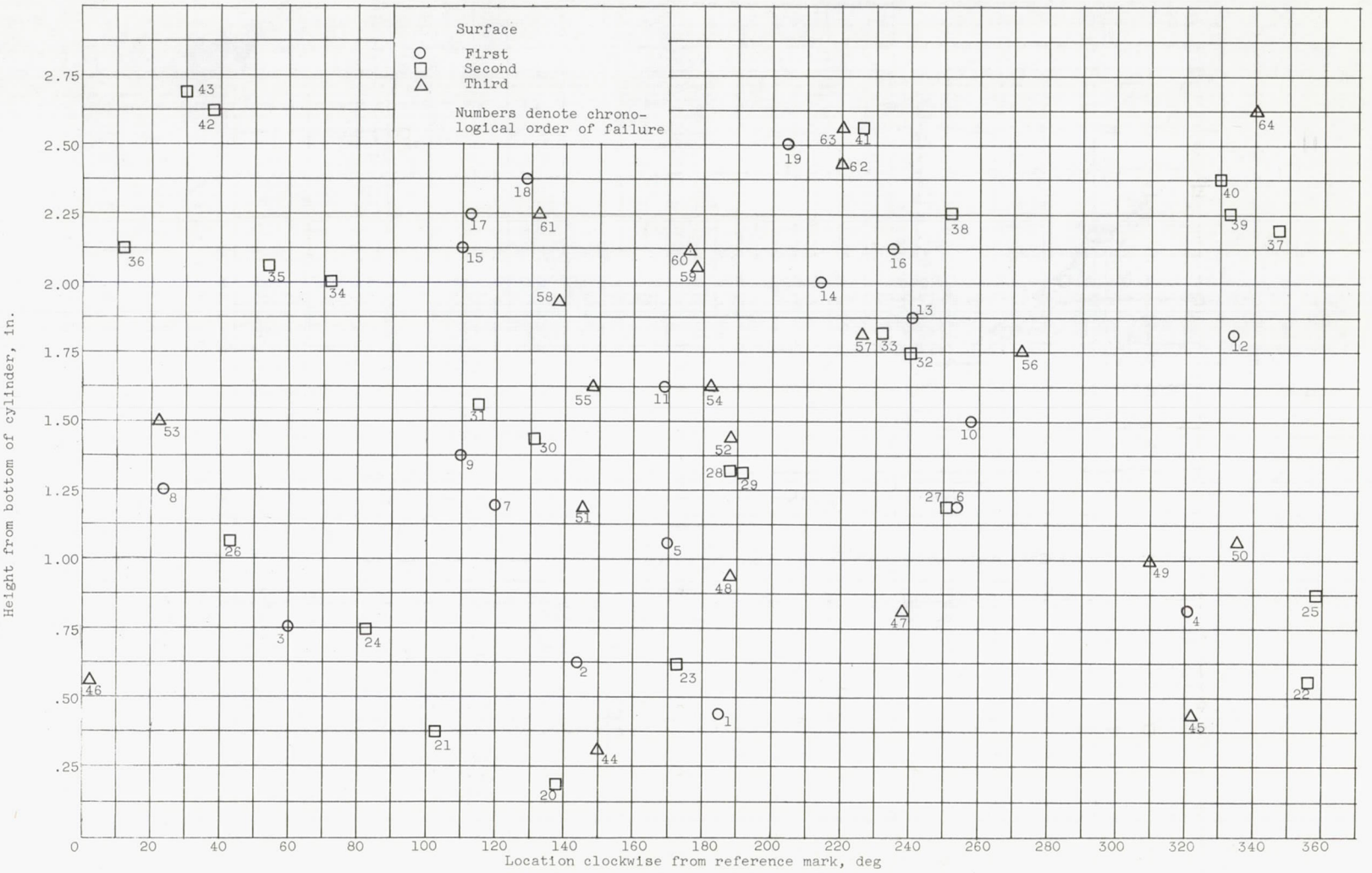

(a) Four quadrants.

Figure 10. - Failure locations in 0° to 45° cylinder.

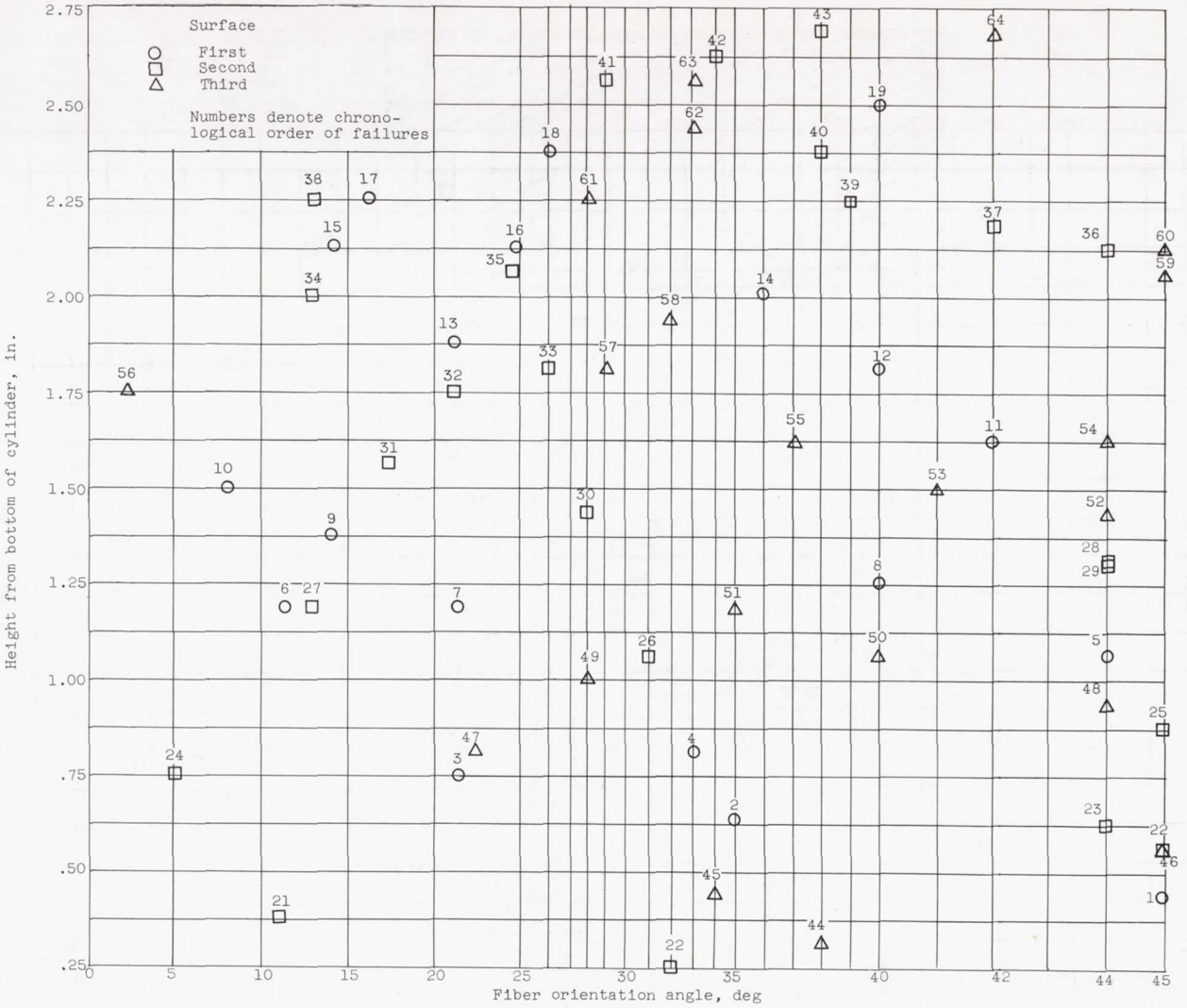

(b) Condensed into an equivalent first quadrant.

Figure 10. - Concluded. Failure locations in 0° to 45° cylinder.

4697

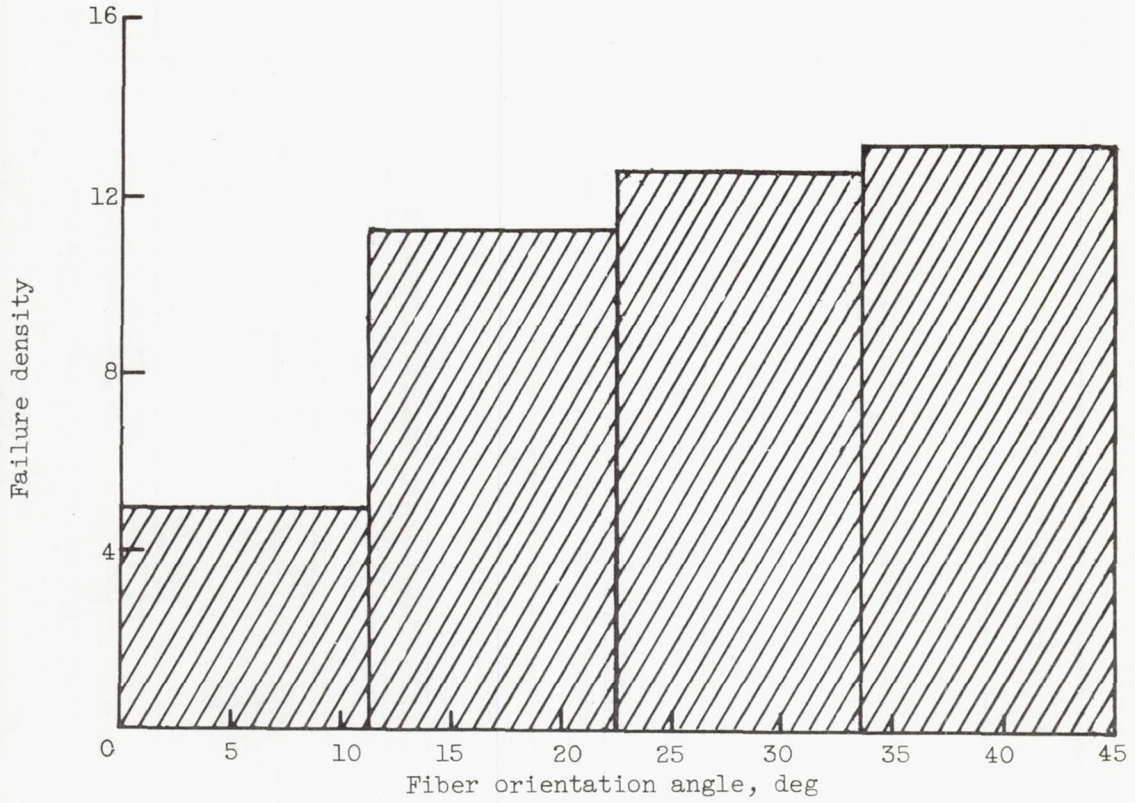

Figure 11. - Distribution of failures in 0° to 45° cylinder (corrected for unequal areas).

4697

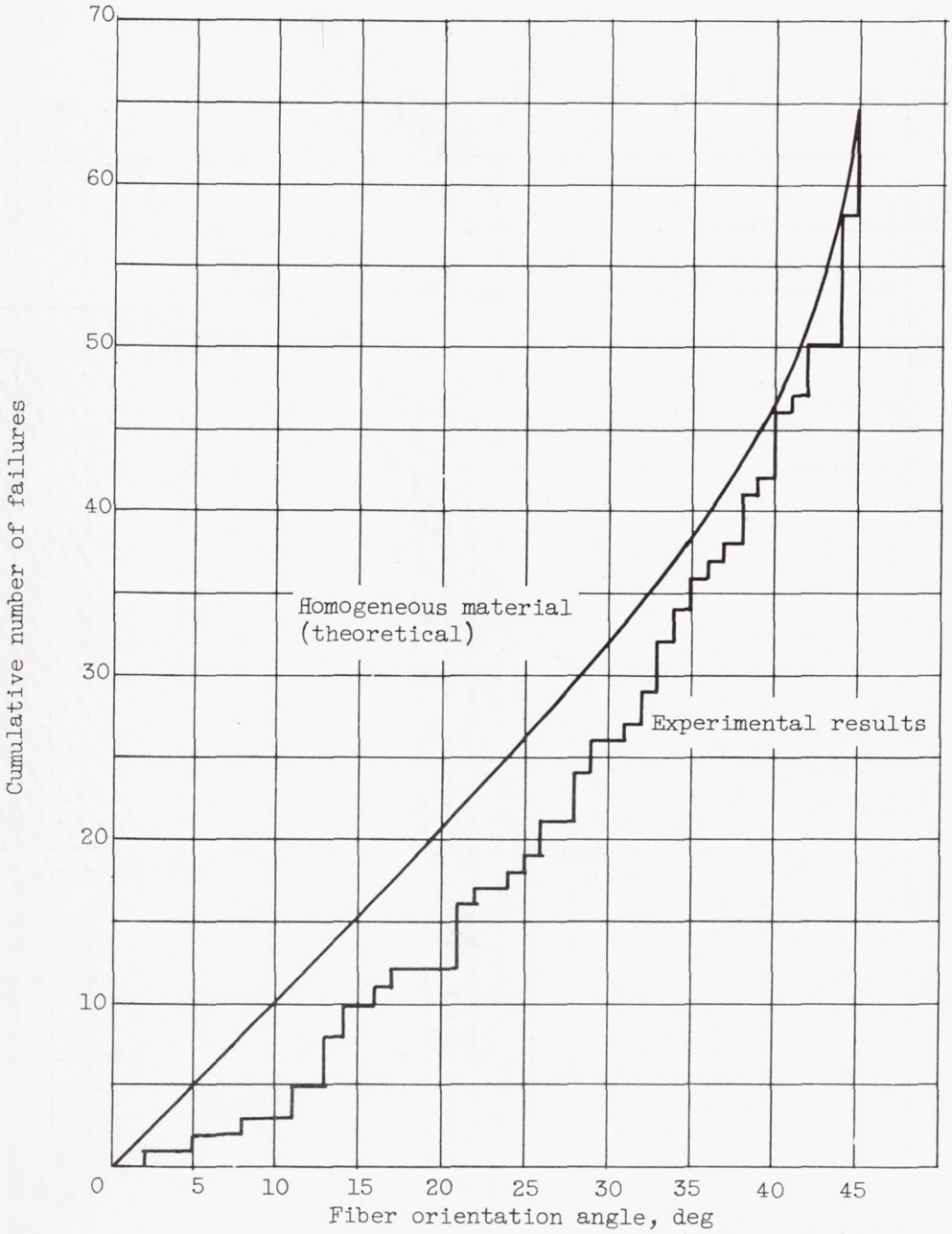

Figure 12. - Cumulative failure distribution in 0° to 45° cylinder.

4697

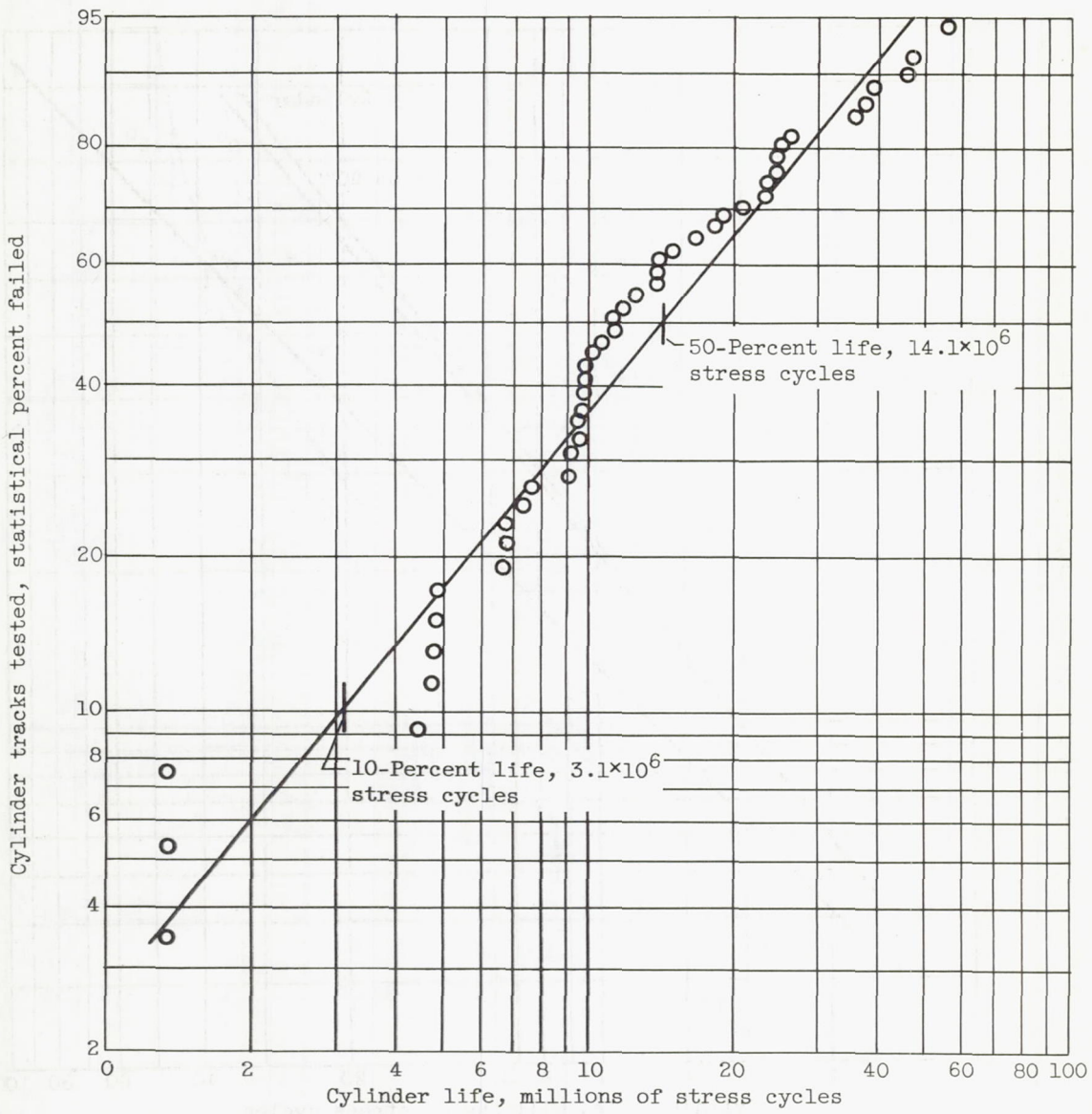

Figure 13. - Fatigue life of 0° to 45° cylinder at room temperature. Lubricant, SAE 10 mineral oil; maximum Hertz compressive stress, 750,000 pounds per square inch.

4697

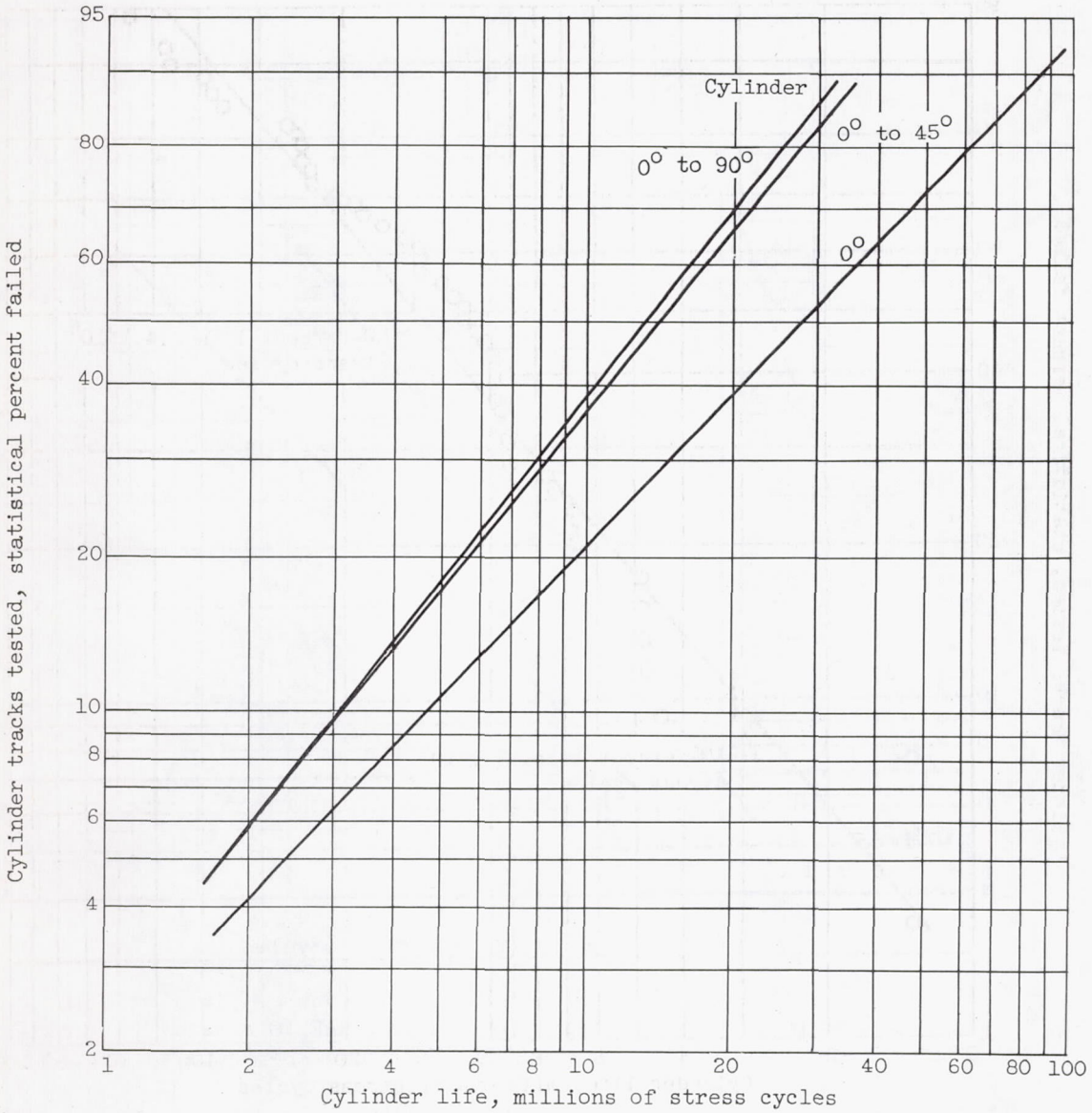

Figure 14. - Summary of fatigue lives of 0°, 0° to 45°, and 0° to 90° cylinders at room temperature. Lubricant, SAE 10 mineral oil; maximum Hertz compressive stress, 750,000 pounds per square inch.

4697

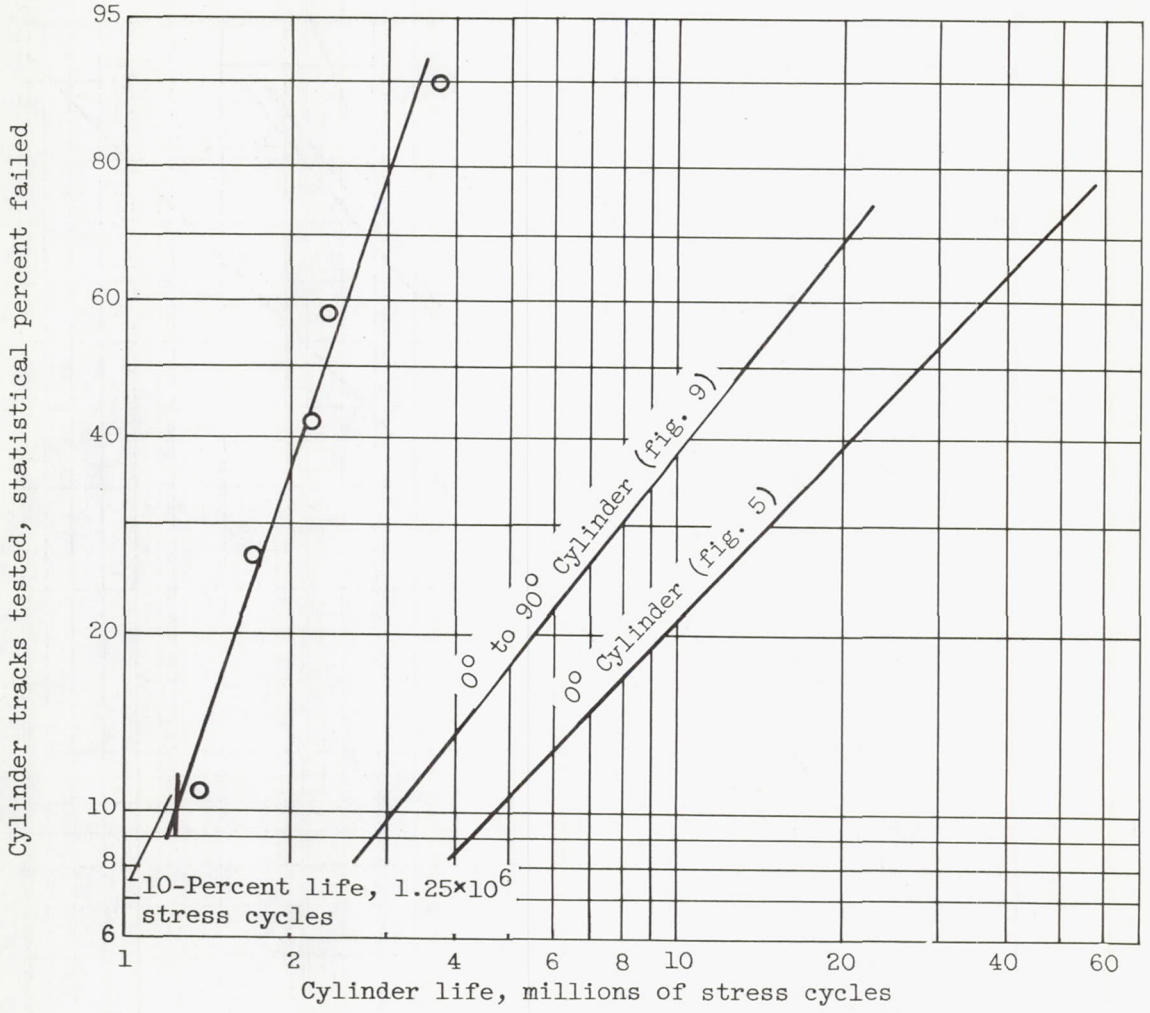

Figure 15. - Fatigue life in the 81° to 90° zone of fiber orientation angles in 0° to 90° cylinder. Lubricant, SAE 10 mineral oil; maximum Hertz compressive stress, 750,000 pounds per square inch.

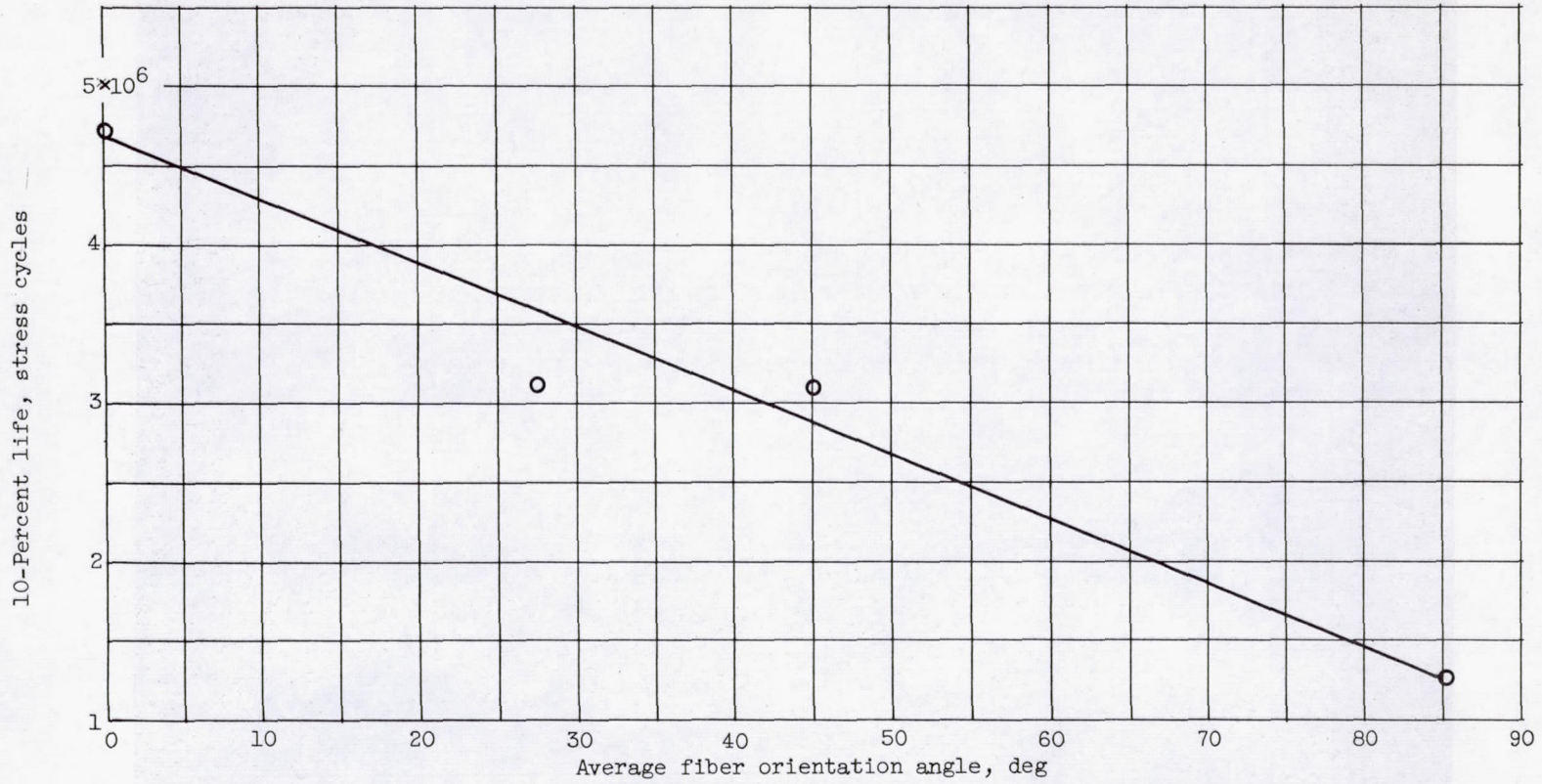

Figure 16. - 10-Percent life as function of average fiber orientation angle.

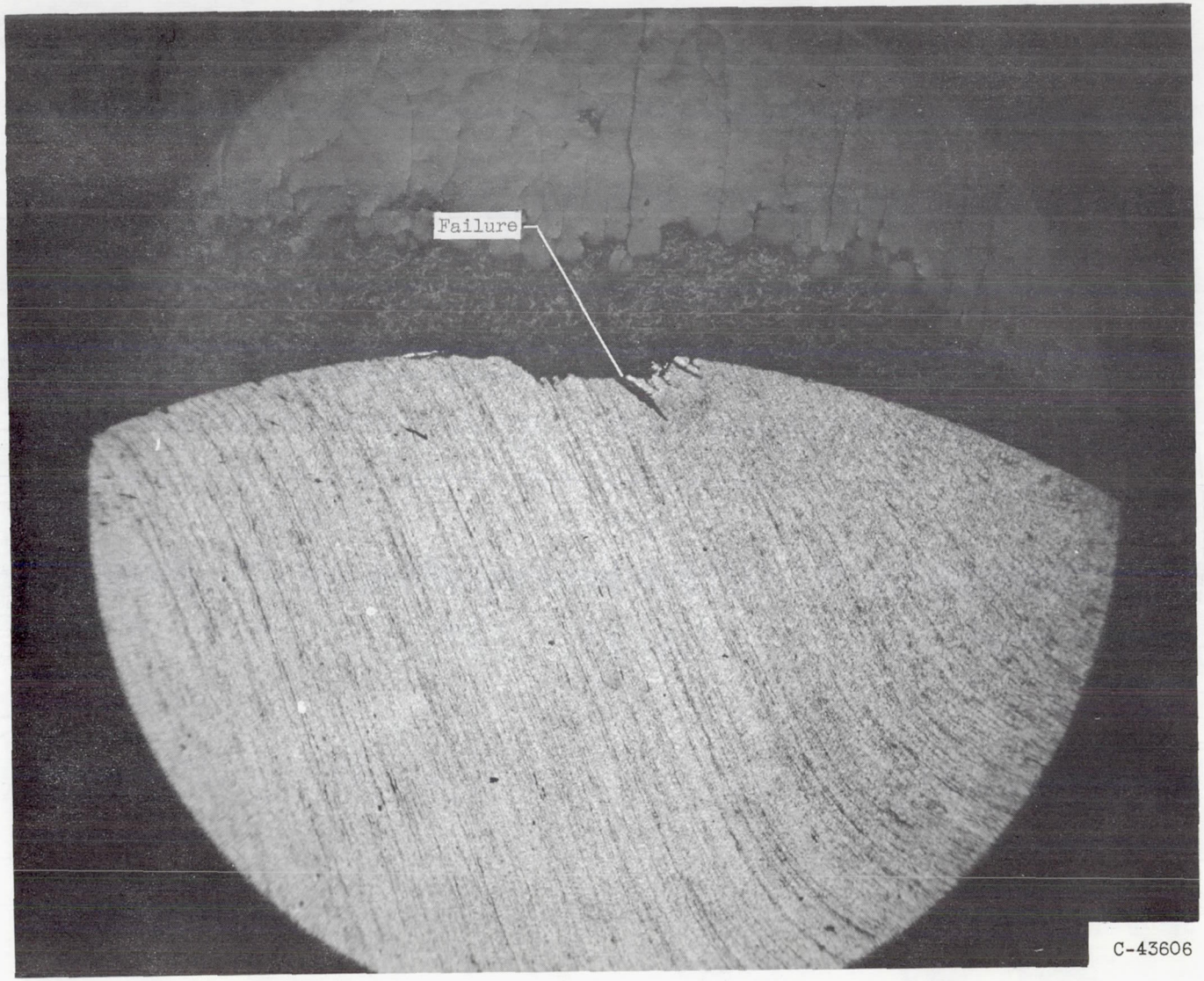

Figure 17. - Pole failure on SAE 52100 ball (sectioned and macroetched).

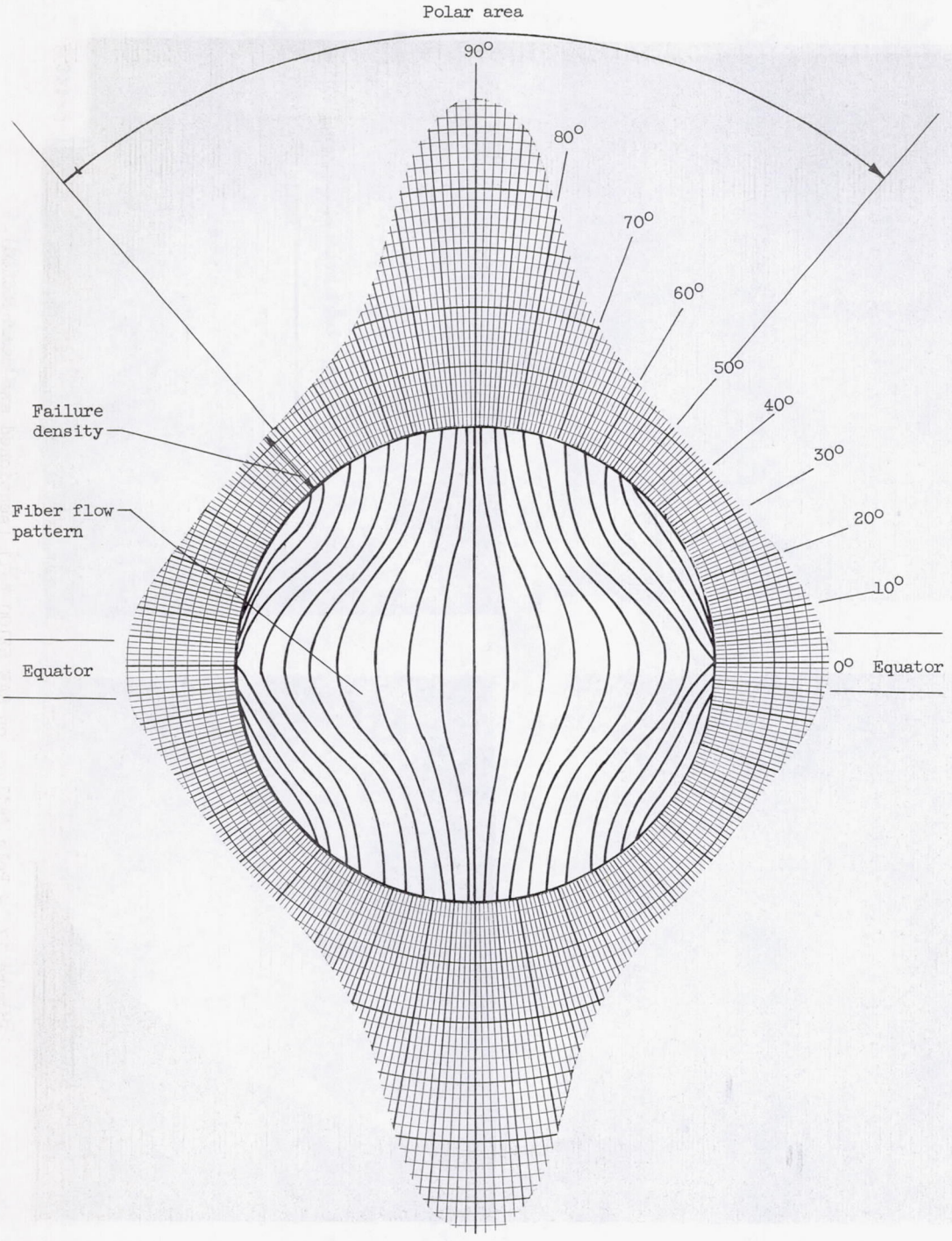

Figure 18. - Failure density as function of ball latitude (for 211 failures and 10 materials).

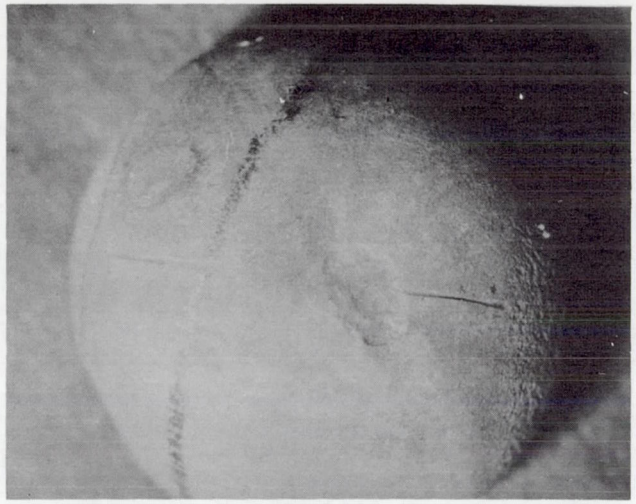

(a) AISI M-10.

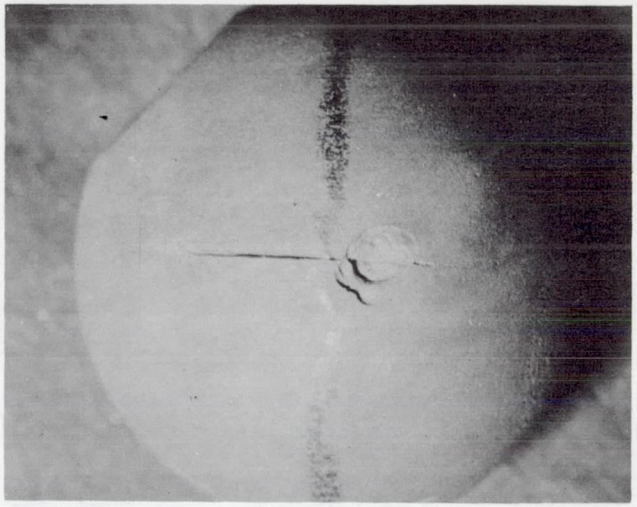

(b) AISI M-1.

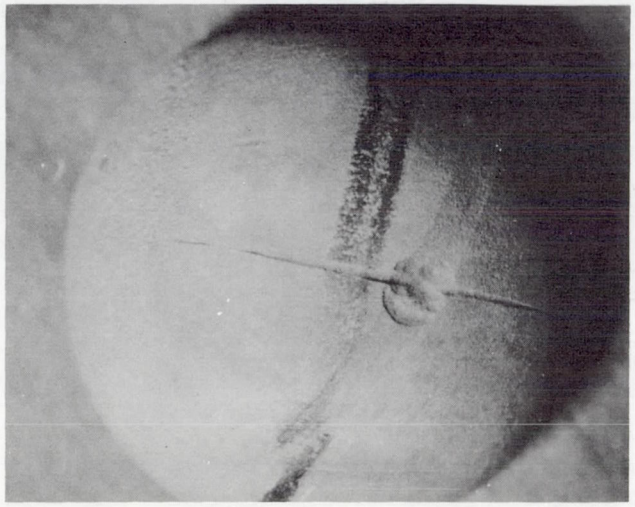

(c) AISI T-1.

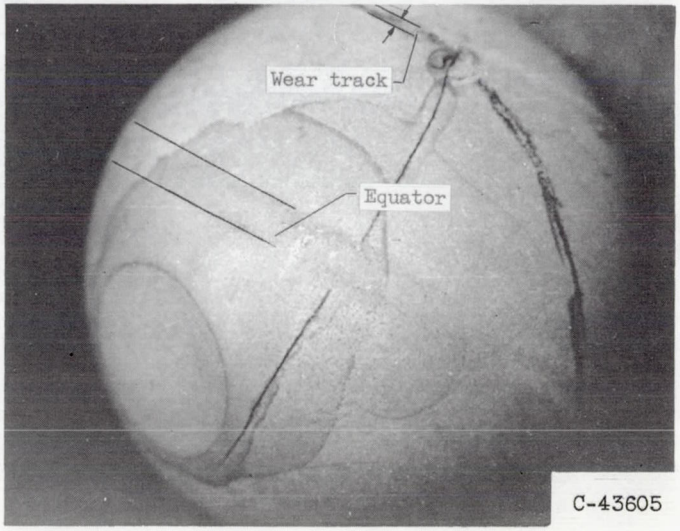

(d) SAE 52100.

Figure 19. - Typical failure-causing inclusions perpendicular to equator and coincident with failure fault line.

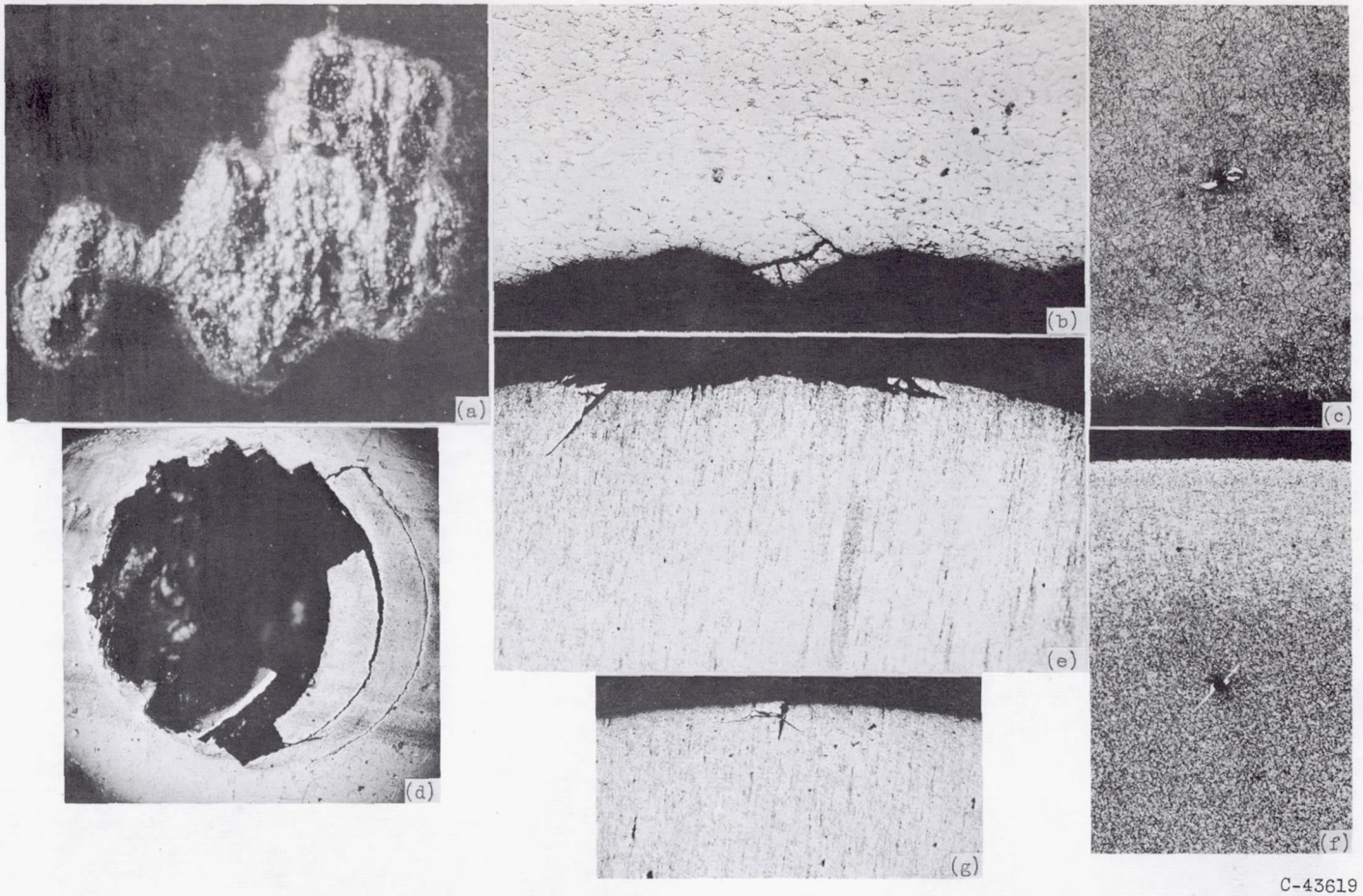

C-43619

(a) Small spall on inner race of M-1 (222) bearing. ×15.
(b) Section view of part of same spall. ×37.
(c) Incipient failure near point of maximum shear stress. ×100.
(d) Typical spalled rig-tested ball. ×50.
(e) Section view of spall. ×37.
(f) Incipient failure near point of maximum shear stress. ×100.
(g) Section view of early failure on rig-tested ball. ×50.

Figure 20. - Comparison of failures of a bearing inner race and balls tested in rolling-contact fatigue spin rig.